AD_____

SPATIAL RELATIONSHIPS BETWEEN DRUG BINDING SITES ON THE SURFACE OF THE ACETYLCHOLINE RECEPTOR

FINAL REPORT

David A. Johnson, Ph.D.

February 13, 1989

Supported by

U.S. ARMY RESEARCH AND DEVELOPMENT COMMAND
Fort Detrick, Frederick, Maryland 21702-5012

Contract No. DAMD17-84-C-4187

University of California, Riverside
Riverside, California 92521-0121

SECURITY CLASSIFICATION OF THIS PAGE

REPORT DOCUMENTATION PAGE

Form Approved
OMB No. 0704-0188

1a. REPORT SECURITY CLASSIFICATION Unclassified	1b. RESTRICTIVE MARKINGS
2a. SECURITY CLASSIFICATION AUTHORITY	3. DISTRIBUTION/AVAILABILITY OF REPORT Approved for public release; distribution unlimited
2b. DECLASSIFICATION/DOWNGRADING SCHEDULE	
4. PERFORMING ORGANIZATION REPORT NUMBER(S)	5. MONITORING ORGANIZATION REPORT NUMBER(S)
6a. NAME OF PERFORMING ORGANIZATION University of California-Riverside 6b. OFFICE SYMBOL (If applicable)	7a. NAME OF MONITORING ORGANIZATION
6c. ADDRESS (City, State, and ZIP Code) Riverside, California 92521-0121	7b. ADDRESS (City, State, and ZIP Code)
8a. NAME OF FUNDING/SPONSORING ORGANIZATION U.S. Army Medical Research & Development Command 8b. OFFICE SYMBOL (If applicable)	9. PROCUREMENT INSTRUMENT IDENTIFICATION NUMBER Contract No. DAMD17-84-C-4187
8c. ADDRESS (City, State, and ZIP Code) Fort Detrick, Frederick, Maryland 21702-5012	10. SOURCE OF FUNDING NUMBERS PROGRAM ELEMENT NO. 62734A; PROJECT NO. 3M1-62734A875; TASK NO. AI; WORK UNIT ACCESSION NO. 457

11. TITLE (Include Security Classification)

Spatial Relationships Between Drug Binding Sites on the Surface of the Acetylcholine Receptor

12. PERSONAL AUTHOR(S)
David A. Johnson, Ph.D.

13a. TYPE OF REPORT	13b. TIME COVERED	14. DATE OF REPORT (Year, Month, Day)	15. PAGE COUNT
Final Report	FROM 9/15/84 TO 9/14/87	1989 February 13	73

16. SUPPLEMENTARY NOTATION

17. COSATI CODES			18. SUBJECT TERMS (Continue on reverse if necessary and identify by block number)
FIELD	GROUP	SUB-GROUP	Acetylcholine receptor, cobra a-toxin, fluorescein isothiocyanate, ethidium, anesthetics, fluorescence, RA V

19. ABSTRACT (Continue on reverse if necessary and identify by block number)

This report describes the preparation and/or characterization of several fluorescent probes of the muscle-type nicotinic acetylcholine receptor for *Torpedo californica*. These probes include the following: (1) four fluorescein isothiocyanate *Naja naja siamensis* α-*toxin 3* derivatives labeled at either lys-23, lys-35, lys-49, or lys-69. (2) a tetramethylrhodamine α-toxin derivative labeled at lys-23. (3) ethidium bromide, and (4) decidium. With these probes and 6-(5-dimethylaminonaphthalene-1-sulfonamido)hexanoic acid β-((N-trimethylammonium)ester (dansyl-$C_6^{\wedge}$-choline) and bis(choline)-N-(4-nitrobenzo-2-oxa-1,3-diazol-7-yl)-iminodiproprionate (BCNI), we estimated the distance between the acetylcholine binding sites and the high-affinity noncompetitive inhibitor site by using fluorescence energy transfer techniques. We, also, estimated the orientation of the snake venom α-toxin bound to the acetylcholine receptor with respect to the central ion channel and the plane of the membrane.

20. DISTRIBUTION/AVAILABILITY OF ABSTRACT ☐ UNCLASSIFIED/UNLIMITED ☐ SAME AS RPT. ☐ DTIC USERS	21. ABSTRACT SECURITY CLASSIFICATION Unclassified
22a. NAME OF RESPONSIBLE INDIVIDUAL Mrs. Virginia M. Miller	22b. TELEPHONE (Include Area Code) 301/663-7325 22c. OFFICE SYMBOL SGRD-RMI-S

DD Form 1473, JUN 86 *Previous editions are obsolete.* SECURITY CLASSIFICATION OF THIS PAGE

FOREWORD

In conducting the research described in this report, the investigators adhered to the "Guide for the Care and Use of Laboratory Animals," prepared by the Committee on Care and Use of Laboratory Animals of the Institute of Laboratory Animal Resources, National Research Council (DHEW Publication No. (NIH) 78-23, Revised 1978).

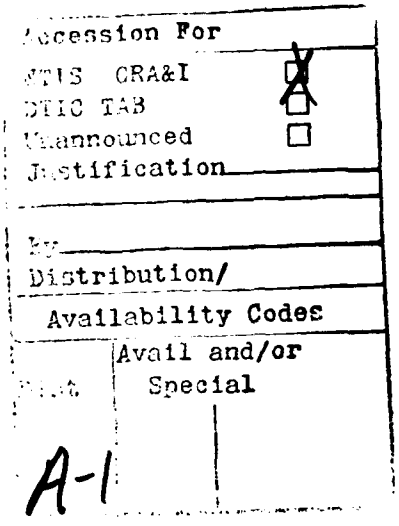

TABLE OF CONTENTS

LIST OF FIGURES

LIST OF TABLES

SECTION I

BACKGROUND

At the molecular level, investigations on the mechanism of action of acetylcholine and other acetylcholine receptor-active drugs at the neuromuscular junction have focused mainly on the electroplax from *Electrophorus electricus* or the various species of *Torpedo* and *Narcine*. Electroplax have been studied due to their exceptional richness in cholinergic synapses. Pharmacologically, the electroplax responds to cholinergic agents like the neuromuscular endplate and, consequently, are considered to be an excellent model of the mammalian neuromuscular-nicotinic synapse [1-3].

Structure of the acetylcholine receptor. The *Torpedo californica* acetylcholine receptor has been the most thoroughly studied of the acetylcholine receptor (AcChR) systems. The AcChR is composed of five subunits, two of which appear to be identical. The subunits are designated α_2, β, γ, and δ and have apparent molecular masses of 40kDa, 49kDa, 58kDa, 64 kDa, respectively [5,6]. Only the α subunits are specifically labeled by affinity-labeling reagents such as bromoacetylcholine or 4-(N-maleimidophenyl)-[^{3}H]-trimethyl ammonium (MBTA), suggesting that the α subunits contain the two acetylcholine or α-neurotoxin binding sites [5,7]. The primary amino acid sequences of the five subunits indicate significant subunit homology [8-10]. Based on the sequences of the subunits, models of the folding of the AcChR have been proposed. Each subunit includes four hydrophobic segments, designated M1 to M4, which could span the bilayer as alpha helices. In addition, each subunit contains a subsequence, designated MA, which may form an amphipathic membrane-spanning helix. (No agreement exists on which segments span the membrane [10,31-36], but the above view appears to be the most prevalent one.)

Negatively stained electron micrographs of the *Torpedo* indicate that the membrane-associated AcChR is shaped like a circular cylinder, 90 ± 10 Å in diameter, and has a central cavity of 15-20 Å in diameter [12]. The electron density profile through receptor-rich membrane fragments shows that the receptor extends ~55 Å out of the plasma side of the bilayer and ~15 Å into the cytosol with an overall length of ~110 Å normal to the plane of the membrane [12]. Because all five subunits span the bilayer, they can be portrayed as staves in a barrel. The arrangement of these staves appears to be $\alpha\beta\gamma\alpha\gamma\delta$ [51].

Ligand binding sites on receptor. Each *Torpedo* receptor contains distinct saturable binding sites for agonists and competitive antagonists [13,14] and for noncompetitive inhibitors (NCIs) [14-16]. There are two sites where agonists and competitive antagonists bind. At least two classes of NCI sites exist: one class (high affinity) binds one molecule of a high-affinity NCI (such as phencyclidine (PCP) or histrionicotoxin (HTX) per receptor and one class (low affinity) binds 10-30 molecules of aliphatic alcohols or other low-affinity NCIs [21-22, 50]. In addition to the stoichiometry of binding, the high- and low- affinity NCIs display disparate Hill slopes. Agents binding to the high-affinity site exhibit unity Hill slopes, while agents binding to the low-affinity sites display greater than unity Hill slopes [50]. This suggests positive cooperativity in the binding to the low-affinity but not to the high-affinity sites.

One focus of current research has been towards the determination of the locations of the important functional domains of the receptor. Agonists and competitive antagonists have been shown to bind to the two α subunits at or near Trp 149, Tyr 190, Cys 192, and Cys 193 [24,25]. Using electron microscopy and single-particle image averaging at ~20 Å resolution, Zinghseim et al. [18] showed that α-bungarotoxin, a competitive antagonist, binds at two regions of the receptor: one adjacent to the δ subunit and the other diametrically across the receptor molecule, ~50 Å away from the δ subunit. This distance has been confirmed by us, using fluorescence energy transfer techniques [20] and more recently by Kubalek, et al., using image analysis of electron micrographs

[52]. The homologous positions in the M2 regions of the α, β, and δ subunits (α 248, β 254, and δ 262) are specifically affinity-labeled by [^{3}H]triphenylmethylphosphonium [26], a high-affinity NCI. This has been confirmed using [^{3}H]chlorpromazine, which binds to the high-affinity NCI site [27,28]. Since high-affinity NCIs specifically label multiple subunits, the site of interaction of the high-affinity NCIs is thought to be in the central channel[26-28]. The location of the high-affinity NCI site in the central channel is also suggested by the kinetics of inhibition by NCIs [35,36].

Research to delineate the molecular details of α-toxin interaction with the AcChR has also included efforts to determine how snake venom α-neurotoxins interact with the receptor. Work toward this goal has (1) examined the effects of chemical modification of discrete sites on the α-toxin [45-47], (2) examined the structural homologies between all α-neurotoxins, (3) compared the structural domains of the α-neurotoxins with the tertiary structure of acetylcholine [43], (4) examined solute and macromolecular accessibility to discrete regions of the α-neurotoxins free in solution and bound to the receptor [24,40] and (5) examined the capacity of synthetic peptides that correspond to subsequences of the α-neurotoxins to bind to the AcChR [41,42].

Use of fluorescent probes. The use of fluorescence techniques requires fluorescent probes with known pharmacological action. Because there were a limited number of fluorescent agents that bind specifically to the receptor, we have spent much of our time during the past eight years preparing and characterizing such agents. For example, we have isolated and characterized four of six possible monoconjugated fluorescein isothiocyanate (FITC)-cobra *Naja naja siamensis α-toxin 3* (α-toxin) derivatives. These derivatives are labeled at lys 23, 35, 49, or 69 [19,53] (See Section II). We have also isolated and characterized a tetramethylrhodamine isothiocyanate (TRITC) lys 23-cobra-α-toxin derivative (see Section III and [54]). We have also determined that ethidium binds to the high-affinity NCI site [39] and, consequently, can be used as to probe the high-affinity NCI site (See Section IV). Moreover, we have characterized the interactions of the receptor with two fluorescent competitive antagonists, decidium[30] and BCNI [37], which can be utilized to study the agonist and competitive antagonists binding sites (see Section V).

SECTION II

CHARACTERIZATION OF FOUR MONOCONJUGATED FITC-TOXINS

Preparation of FITC-labeled α-Toxins. To redirect the FITC labeling away from the hyperreactive α-toxin lys 23, we reversibly modified α-toxin with citraconic anhydride. The modified α-toxin was then labeled with near- stoichiometric quantities of FITC, treated with acid to remove the citraconic anhydride, dialyzed, concentrated, and focused in one pH unit (9.0-10.0 to 9.3-10.3) IPG gels. The left panel of Fig. 1 shows a fluorescence photograph of one of these gels and a density scan of the photograph negative. Five, and sometimes six consistently spaced fluorescent bands focused between the cathode and anode and are referred to as Bands 1 to 6, respectively. Poly-FITC- conjugated α-toxins and monoconjugated FITC focused at the anode, while native α-toxin focused at the cathode (data not shown). Some tailing appeared from Band 6 into adjacent Bands 4 and 5. We could not determine the pH gradient of the gels, because the pH gradient is maintained by a modification of the poly acrylamide gel. Consequently, efforts to measure the pH of homogenized serial sections of the gel or to utilize a surface pH electrode were unsuccessful. We estimated the pIs of Band 1 and 6 to be ~9.3 and ~9.6, respectively, because we previously observed [19] that on an isoelectrofocusing column mono-FITC-toxin derivatives focus between pH 9.3 and 9.6.

Sufficient material was associated with the FITC-toxin monoconjugate Bands 1, 2, 3, 5, and 6 to attempt isolation and sequencing. These bands were extricated from the gel by adsorption onto cation exchange resin. The monoconjugates were eluted from the resin with a high ionic strength buffer. Significant amounts of glycerol and other gel contaminants from the IPG gel eluted with the mono-FITC derivatives, even when the gel-resin mixture was placed in a column and eluted with shallow salt gradient (data not shown). Consequently, the mono-FITC derivatives were purified further by reverse phase HPLC. Elution profiles of fluorescence of Bands 1, 2, 3, and 6 and the elution profile of 280 nm extinction of native α-toxin are shown in Fig. 2. Although our HPLC protocol did not resolve all the mono-FITC derivatives, native α-toxin eluted before the FITC-toxins and band 6 eluted before Bands 2, 3, and 5. (Band 5 profile not shown). Consequently, trace native α-toxin and Band 6 contaminates were removed from Band 2, 3, and 5 samples. To estimate final purity, the HPLC-purified Bands 1, 2, 3, and 6 were focused on an IPG. Based on fluorescence, Bands 1, 2, 3, and 6 were greater than 95% pure (Right Panel, Fig. 1). Band 5, though chromatographically homogeneous on IPG and reverse phase HPLC systems described above, is not shown because microsequencing indicated that Band 5 contained more than one mono-FITC derivative.

Protein Recovery. In separate experiments the recoveries of known amounts of FITC-toxin from the IPG gel and the HPLC column were determined to be 71 and 73 %, respectively (data not shown). Also, by separation of FITC-labeled from unlabeled α-toxin with HPLC, we determined that 35% of the α-toxin was labeled after the citraconic anhydride treatment and 68% without citraconic anhydride treatment (data not shown).

The effect of citraconic anhydride modification on the pattern of FITC monolabeling was estimated from density scans of photograph negatives of the IPG and corrected for quantum yield and extinction of the Bands. These results are summarized in Table I. Citraconic anhydride modification reduced the labeling of Band 6 (from 85 to 68%) and increased the labeling of Bands 1 to 5. The labeling of Band 1 showed the greatest percent increase (from 7 to 20%).

Identification of Sites of Labeling. Bands 1, 2, 3, and 5 were reduced, S-carboxymethlyated, digested with thermolysin, and resolved on a C_{18} reverse phase HPLC. Elution profiles of digests of Bands 1, 2, and 3 on a C_{18} reverse phase column showed only one major fluorescent peak (Figs.

3-5). Sequencing of the fractions associated with the major fluorescent peptide of Band 2 yielded an unambiguous sequence with a linear log recovery versus cycle number plot to be arg-"blank"-arg-pro. A "blank" represented a cycle with no detectable amino acid and suggested the presence of N^{ϵ}-FITC-lys, since N^{ϵ}-FITC-lys did not elute from the sequencing column with the solvent gradients used. (This was further supported by the sequencing of FITC-conjugated polylysine. Only lys was detected off of the column, data not shown). The uniqueness of the arg-"blank"-arg-pro sequence to the region about lys 69 suggests the site of labeling of Band 2 to be lys 69. The peak fluorescent fractions of digests of Bands 1 and 3 were rechromatographed on a C_4 reverse phase column to remove nonfluorescent peptides, that made sequencing equivocal. The rechromatographed fluorescent peaks also displayed single major peaks of fluorescence suggesting homogeneity of the fluorescent peptides associated with the digests of Bands 1 and 3. Sequencing of the fluorescent fractions associated with the rechromatographed major fluorescent peaks from the digestion of Bands 1 and 3 yielded unambiguous sequences with linear log recovery versus cycle number plots of ile-arg-gly-"blank"-arg and val-"blank"-gly, respectively (Top Panel, Figs. 3 and 5). The uniqueness of these sequences in the α-toxin sequence (Fig. 6) suggests that Band 1 was labeled at lys 35 and Band 3 at lys 49. Elution profiles of digests of Band 5 showed at least two major fluorescent peaks eluted from a C_{18} column based on seven determinations. The sequence of one of the fluorescent peptides of Band 5 suggested labeling at lys 12. The other major peak of fluorescence could not be sequenced and suggested that the N-terminus was blocked. These results indicated that Band 5 was a mixture of α-toxin labeled at lysine 12 and at the N-terminus (ile 1). Because we were unable to resolve these derivatives, we focused our attention on characterizing only the isolated mono-FITC derivatives (Bands 1, 2, 3, and 6).

The site of labeling of Band 6 was determined to be lys 23 because Band 6 displayed essentially identical chromatographic, spectroscopic, and binding kinetic properties as our previously identified FITC-lys-23-toxin [19]. Band 6 and FITC-lys-23-toxin focused at the same pI on a 9.0-10.0 IPG gel and displayed the same retention time on reverse phase HPLC (data not shown). The absorbance and emission maxima in NaCl-phosphate buffer (pH 7.4) were identical, 494 and 519, respectively. Both Band 6 and FITC-lys-23-toxin showed the same magnitude of fluorescence enhancement upon binding to the AcChR, 95 and 96%, respectively (Table II; [19]). The quantum yields and molar extinction coefficients of Band 6 and FITC- lys-23-toxin also were essentially identical, .18 versus .16 and 62,000 versus 55,000 $M^{-1}s^{-1}$, respectively (Table II and [19]). Finally, the association rate constants of Band 6 (15×10^3 $M^{-1}s^{-1}$) and FITC-lys-23-toxin (6.7×10^3 $M^{-1}s^{-1}$) were within a factor of two of one another, and the dissociation rate constants differed by less than 6% (3.5×10^{-5} versus 3.3×10^{-5} s^{-1}, respectively) (Table III and [55]).

Spectral Characterization. The absorption spectra and fluorescence emission spectra of the four isolated mono-FITC derivatives free in solution and bound to the AcChR are shown in Fig. 7 and summarized along with the molar extinction, quantum yield, and fractional change of fluorescence upon binding of each isolated monoconjugate in Table II. With the exception of the quantum yields and fractional changes of fluorescence associated with AcChR binding the spectral properties of the FITC- lys-69-, lys-35-, lys-49-, lys-23- α-toxins do not differ greatly. The quantum yields of each of the mono-FITC derivatives are at least half of fluorescein in 0.1 N NaOH (Q=0.85, [56]). The lys-69 derivative displays the highest quantum yield of the four examined, 0.41, and the lys-23 derivative the lowest at 0.18. The fractional changes in fluorescence (excitation at 480nm) associated with binding to the AcChR measured by interpolating to infinite AcChR-toxin sites (Fig. 10) showed the fluorescence of the lys 35, lys 69, and lys 49 to decrease upon binding to the receptor, 39, 26, and 6 %, respectively. In contrast, the fluorescence of the lys 23 derivative increased 96% upon binding to the receptor. When samples are radiated with 280 nm light to maximize the signal from the bound fluorophore, the spectral overlap between receptor tryptophanyl

emission and fluorescein absorbance in the 520 nm band resulted in enhancement of fluorescence of FITC- lys- 23, 35, 49, and 69-toxins (data not shown).

Kinetics of isolated FITC-toxins Binding to the AcChR. As mentioned above the binding of the isolated FITC-toxins with the AcChR is associated with either decreases or increases in fluorescence. Typical recordings of the changes in fluorescence (excitation 480 nm) of FITC-lys-69-, lys-35-, lys-49-, and lys-23 -toxins upon association to the membrane-associated AcChR are shown in Fig. 8. Incubation of excess native α-toxin with AcChR before the addition of FITC-toxins showed no significant changes in fluorescence and demonstrated the ligand-specific nature of these spectral changes. The dissociation rate constants were determined by monitoring the changes in fluorescence after the addition of excess native α-toxin to a solution of FITC-toxin-AcChR complexes (Data not shown). Kinetic rate constants were derived from the slopes of plots of integrated rate expressions for bimolecular association and unimolecular dissociation. Examples of fits to the bimolecular association rate expressions are shown in Fig. 8, and Table III summarizes the kinetic results. As we previously observed with the FITC-lys-23-toxin, the association kinetics of FITC- lys-35-, lys-49-, and lys-69 -toxins could be fit by a bimolecular reversible mechanism and the dissociation kinetics by a unimolecular mechanism. Within a factor of two, the average apparent bimolecular rate constants were independent of the reactant concentration ratio which ranged between 0.5 and 4. This further supports a simple reversible bimolecular inter action of the mono-FITC derivatives and the AcChR. All of the isolated mono- FITC-toxin derivatives bind to the AcChR with between 10 and 115- fold less affinity than native α-toxin. FITC-conjugation affected association more than dissociation. The association rate constants of FITC-lys -69-, -35-, -49-, and, -23 -toxins are reduced 20-, 13-, 29- and 33-fold, respectively. The dissociation rate constants were less affect by the FITC-conjugation. No more than a 5.4-fold reduction was observed (Table III).

Fig. 1. Fluorescence photograph of FITC-toxin reaction mixture and mono-FITC derivatives resolved on IPG gels.

Left Panel: the photograph and optical density scan of the photograph negative of FITC-a-toxin reaction mixture (2.5 μmol α-toxin) resolved on a 5 mm thick gel. Right Panel: fluorescence photograph of isolated FITC-lys 35-toxin (Band 1; 5 nmol) , FITC- lys 69-toxin (Band 2; 5 nmol), FITC-lys 49-toxin (Band 3; 2.7 nmol), and FITC- lys 23-toxin (Band 6; 2.5 nmol) resolved on a 2 mm thick IPG gel. Using the LKB Application Notes No. 324 the pH range of this gel was set between 9.0 and 10.0.

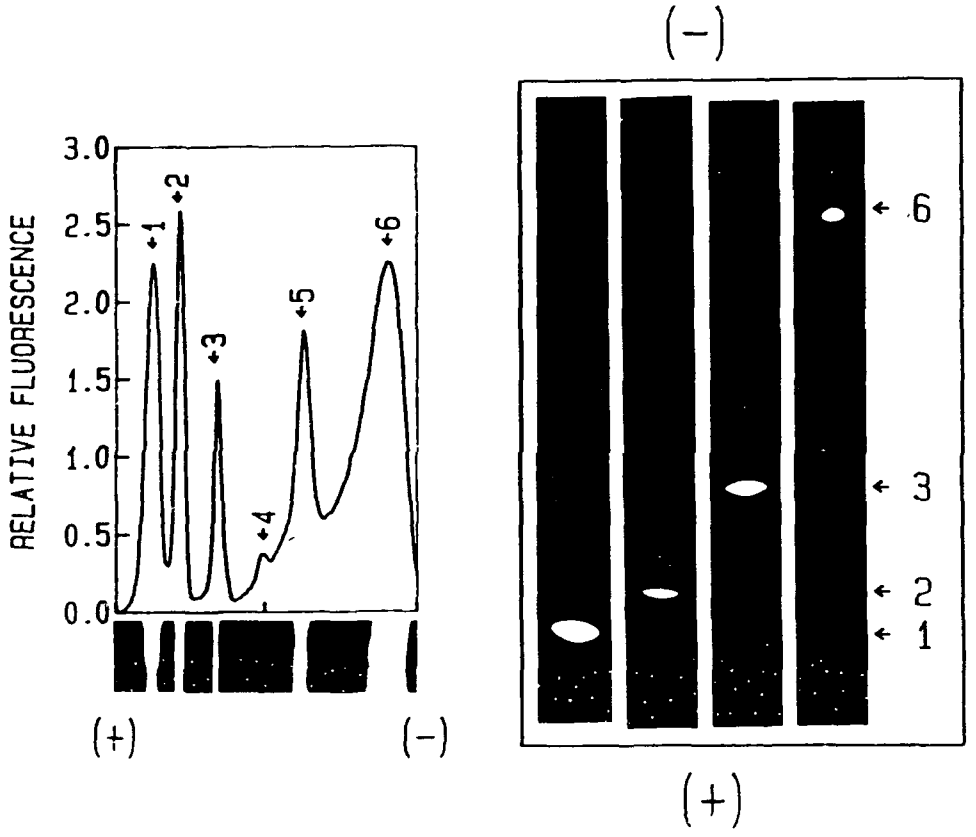

Fig. 2. HPLC elution profiles of mono-FITC derivatives extracted from the IPG gel and native α-toxin.

A: Band 1; B, Band 2; C, Band 3; D, Band 6; E, native α-toxin. The peptides were resolved on a C_{18} column with a linear 80-min gradient of 20 to 40% acetonitrile against 0.1% (w/v) TFA in H_2O. Panels A-D show the elution pattern of FITC fluorescence (EX: 480; EM: 520 nm). Because fluorescein does not fluoresce in low pH, aliquots (20 μl) of the fractions were mixed with 100 mM $NaPO_4$, pH 7.4, to raise the pH. Panel E shows the elution profile of α-toxin monitored at 280 nm.

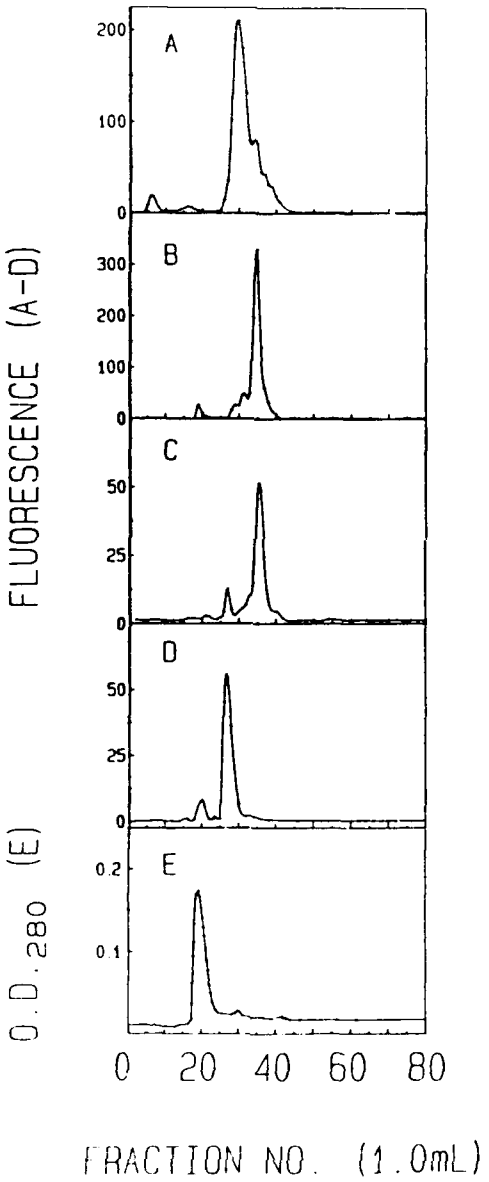

Fig. 3. HPLC elution profile of the thermolysin digestion of the Band 1,FITC-toxin monoconjugate extracted from the IPG gel described in Fig. 1.

Upper Panel, peptide map of total digest resolved on a C_{18} column (0-40% acetonitrile); Lower Panel, resolution of the major peak of fluorescence peak shown in the upper panel on a C_4 column (20-35% acetonitrile); Solid line, 219 nm extinction; dotted line, relative fluorescence.

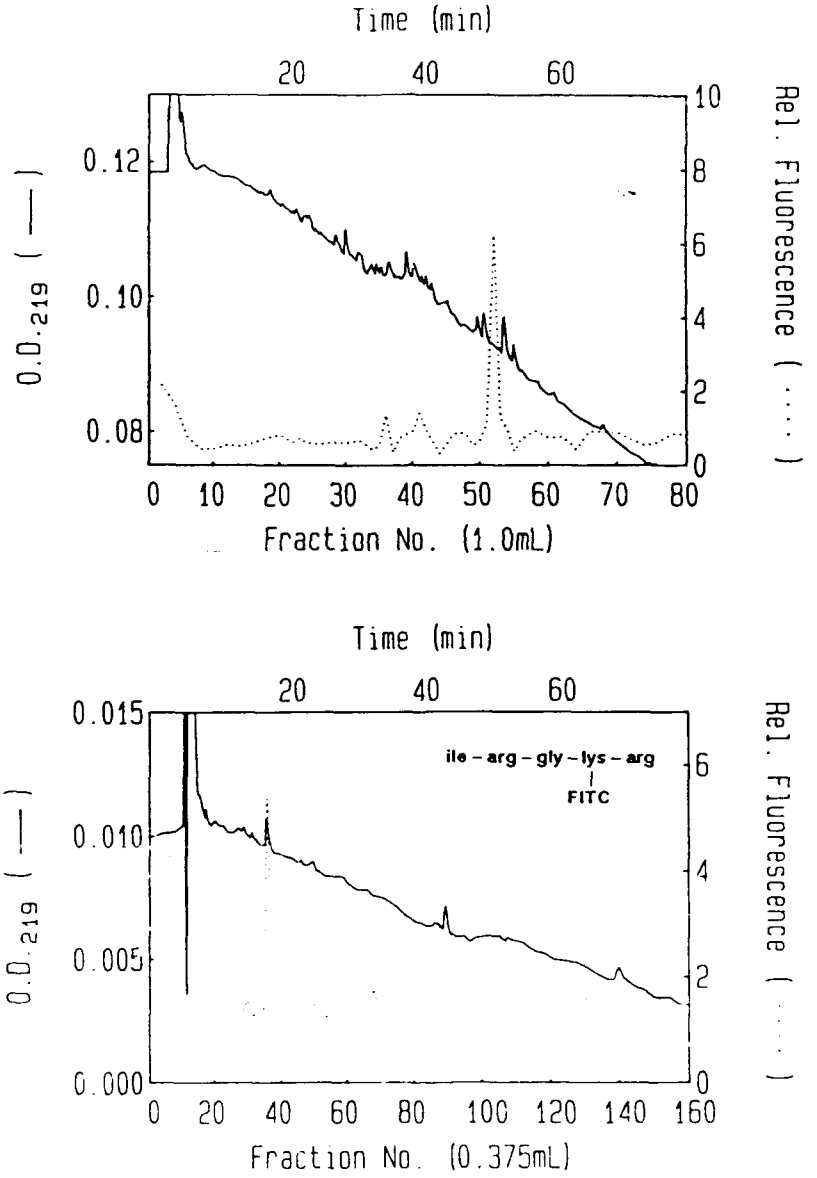

Fig. 4. HPLC elution profiles of the thermolysin digestion of Band 2 FITC-toxin monoconjugate extracted from the IPG gel described in Fig. 1.

Peptide map of total digest resolved on a C_{18} column (0-40% acetonitrile). Solid line, 219nm extinction; dotted line, relative fluorescence.

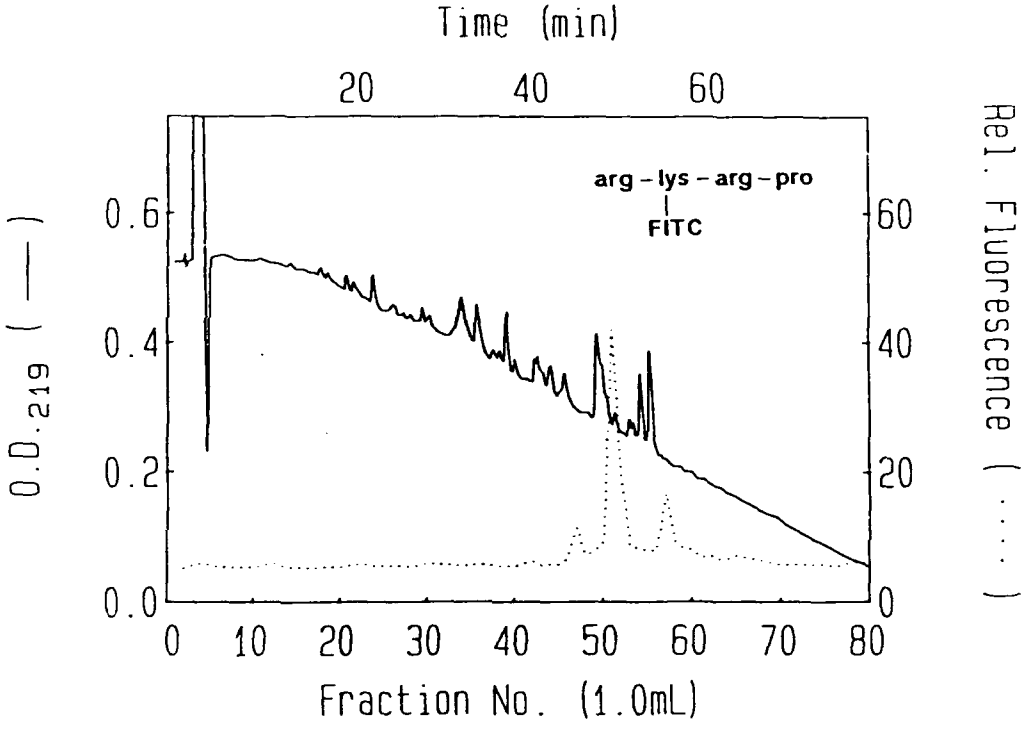

Fig. 5. HPLC elution profiles of the thermolysin digestion of Band 3 FITC-toxin monoconjugate extracted from the IPG gel described in Fig. 1.

Upper Panel, total digest resolved on C_{18} column (0-40% acetonitrile). Lower Panel,major fluorescent peak in upper panel resolved on a C_4 column (20-35% acetonitrile). Solid line, 219nm extinction; dashed line, relative fluorescence.

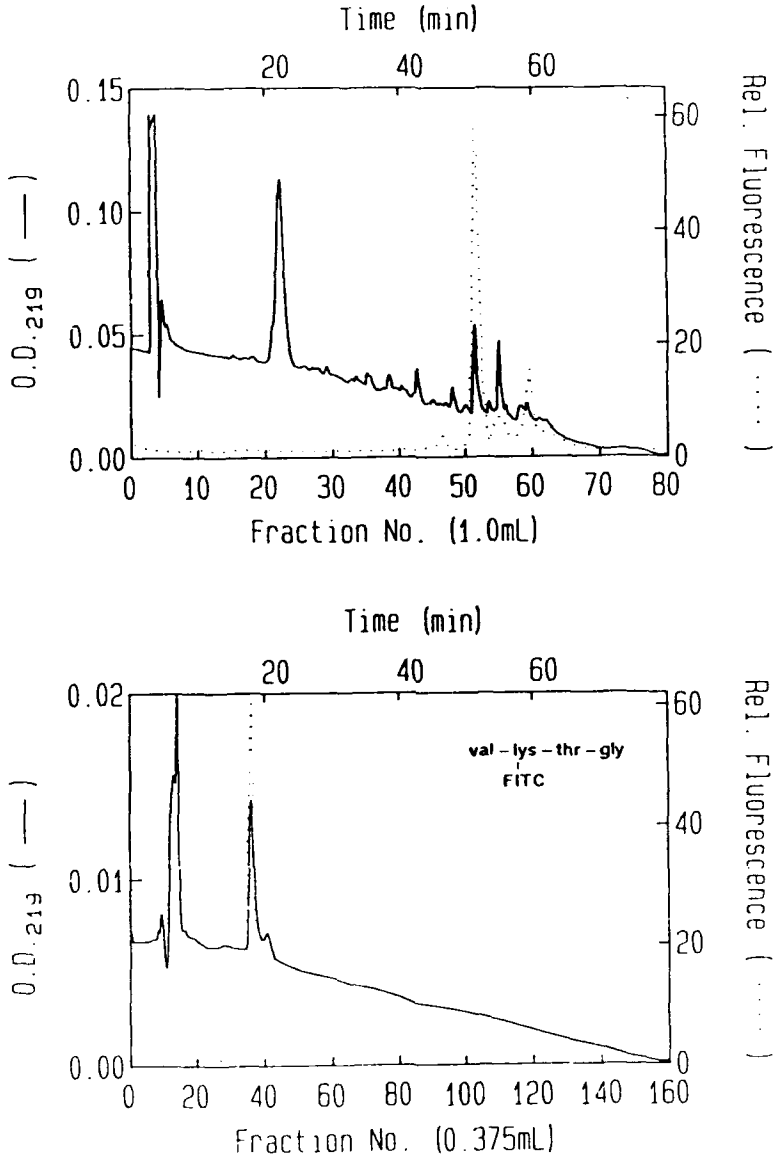

Fig. 6. Sequence of *Naja naja siamensis α-toxin 3.*

Arrows mark sites of labeling.

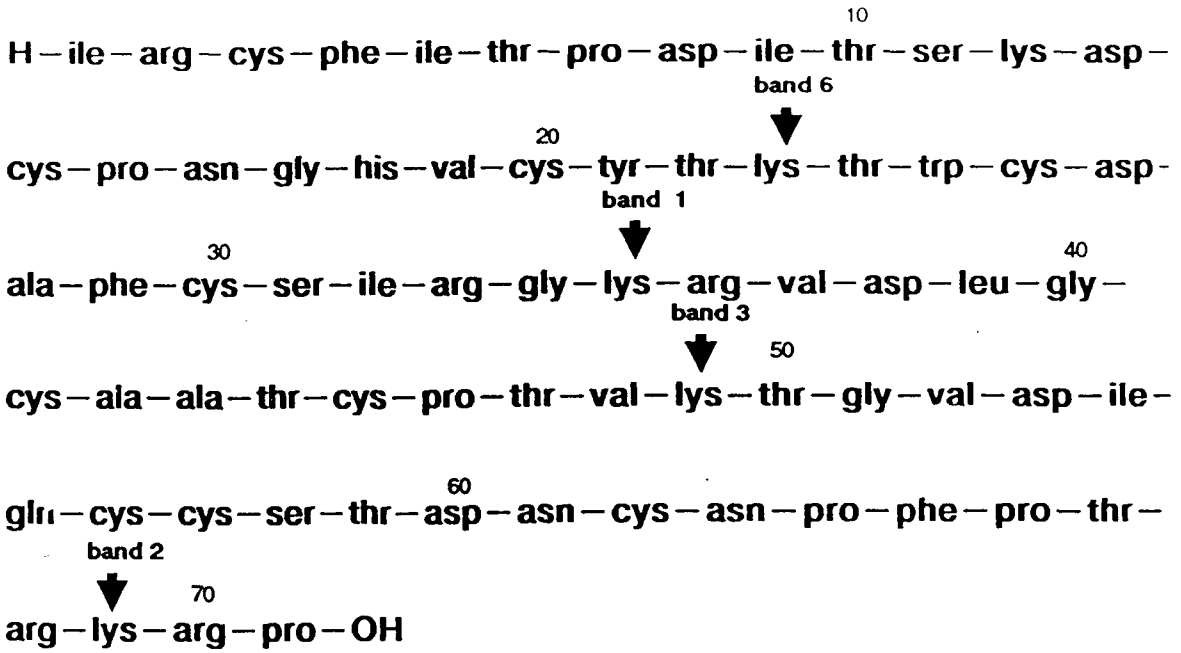

Fig. 7. The extinction (solid line) and fluorescence emission (excitation at 450 nm) spectra of the mono-FITC derivatives in the presence (dashed line)and absence (dotted line) of membrane-associated AcChR (100 nM in α-toxin sites).

Panel A, FITC-lys-35-toxin; Panel B, FITC-lys-69-toxin; Panel C, FITC-lys-49-toxin; Panel D, FITC-lys-23-toxin.

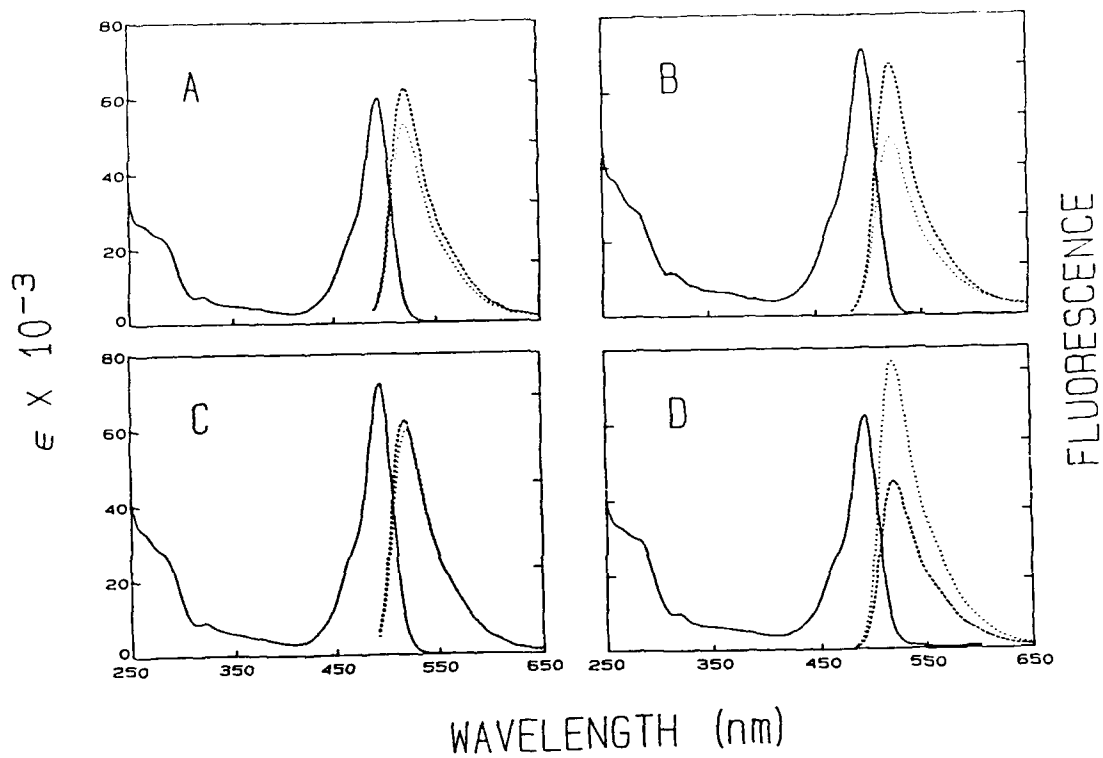

Fig. 8. The association of mono-FITC derivatives (20 nM) with the AcChR toxin sites (80 nM in α-toxin sites).

Shown are the binding-dependent changes in fluorescence (excitation at 480nm, emission at 520 nm). Control rates are measured in the presence of 100nM native α-toxin. Panel A, FITC-lys-35-toxin; Panel B, FITC-lys-69-toxin; Panel C, FITC-lys-49-toxin; Panel D, FITC-lys-23-toxin.

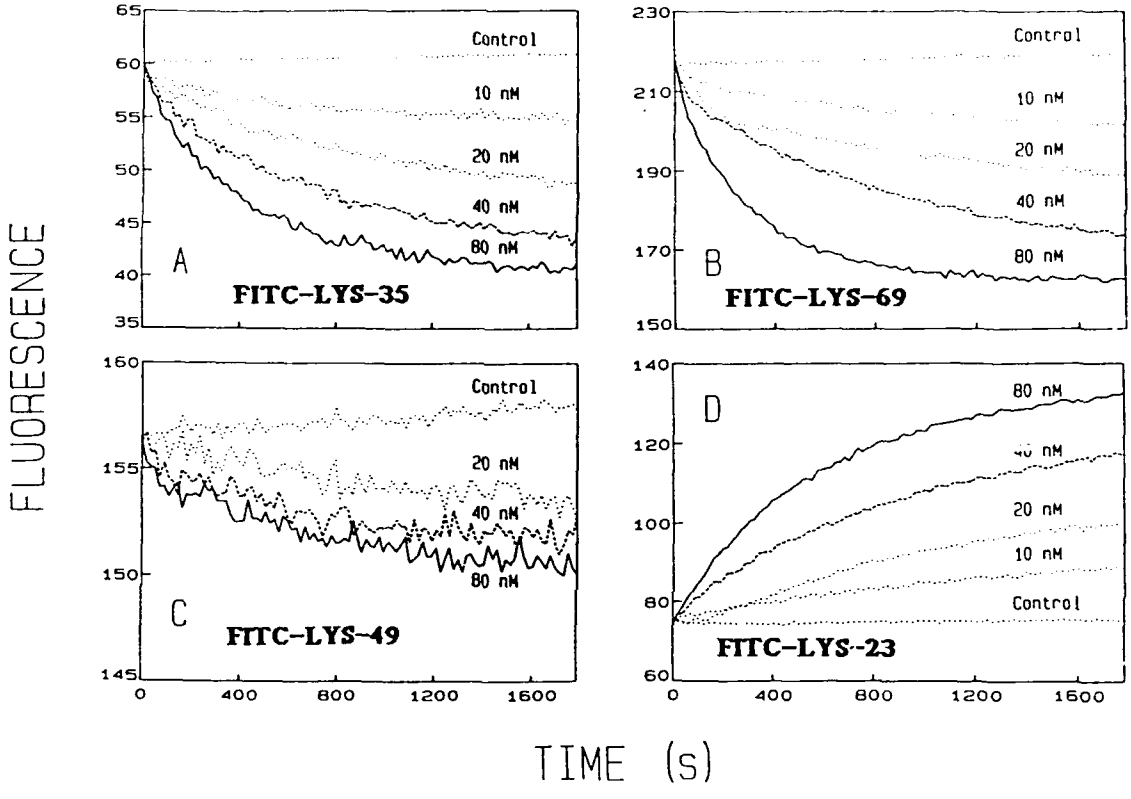

Fig. 9. Integrated rate plots of the binding (20 nM FITC-toxin and 40 nM AcChR in α-toxin sites) reaction fit to reversible bimolecular association mechanism.

Panel A, FITC-lys-35-toxin; Panel B, FITC-lys-69-toxin; Panel C, Panel D, FITC-lys-49-toxin; FITC-lys-23-toxin.

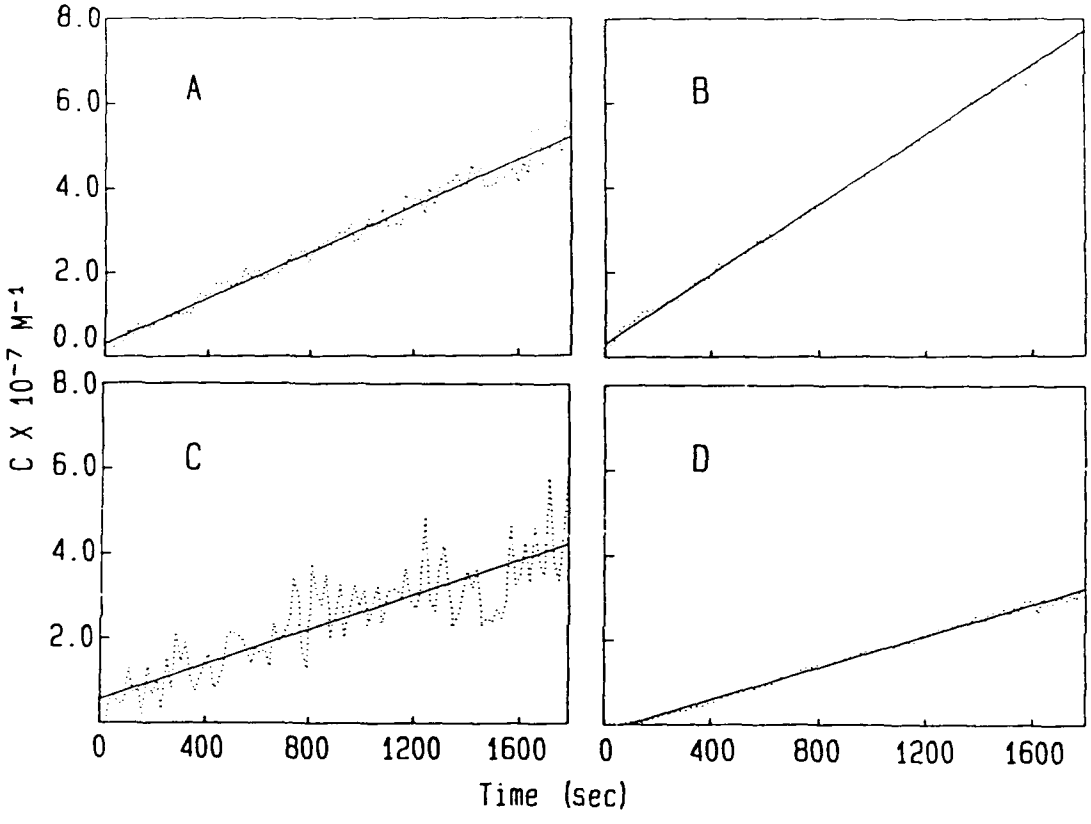

Fig. 10. Determination of the ratio of fluorescence intensity for free and bound species.

Plot of the ratio of fluorescence of FITC-Toxin monoconjugates (20 nM) at equilibrium (I_e) with AcChR and free in solution (I_f) as a function of 1/[AcChR α-toxin sites]. Panel A, FITC-lys-35-toxin; Panel B, FITC-lys-69-toxin; Panel C, FITC-lys-49-toxin; Panel D, FITC-lys-23-toxin.

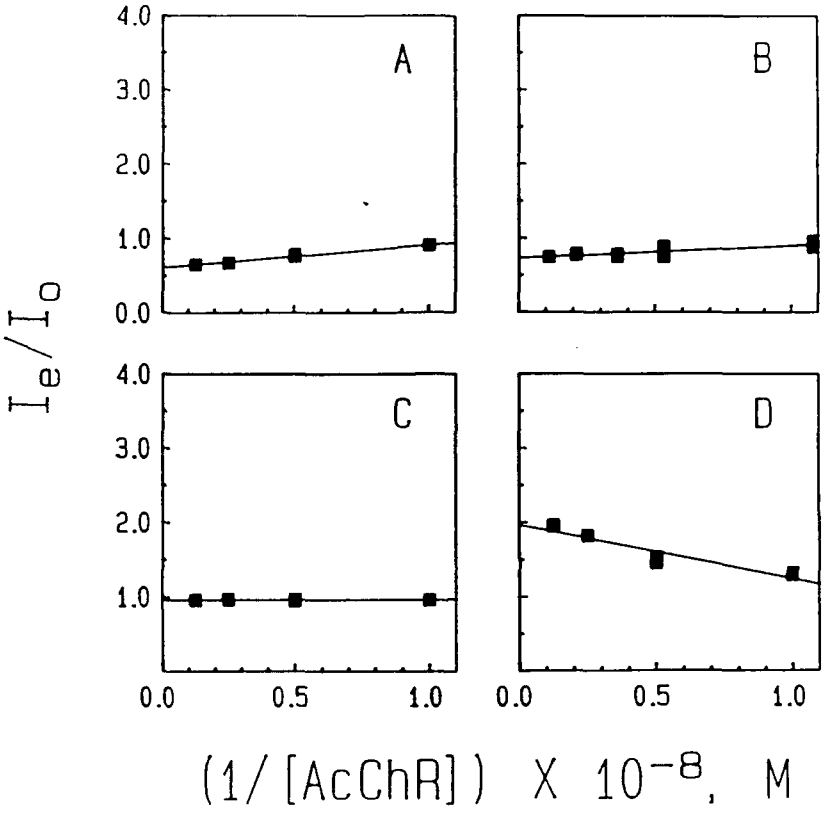

Table I

Effect of citraconic anhydride treatment on FITC labeling of α-toxin.

Values represent fractional estimates of mono-FITC toxins resolved on IPG gels. Quantitation of the bands was achieved by photographing UV illuminated gels, scanning the negatives with a LKB UltroScan XL Laser Densetometer, and integrating the areas under each band. Corrected values represent correction for the quantum yield and extinction using values determined when isolated bands were suspended in 100 mM NaCl, 10 mM $NaPO_4$, pH 7.4 (n.d. = not detectable).

	w/ citraconic anhydride		w/o citraconic anhydride	
	Uncorrected	Corrected	Uncorrected	Corrected
Band 1	.27	.20	.11	.07
Band 2	.11	.06	.10	.05
Band 3	.04	.03	.01	.01
Band 4	>.01	--	n.d.	n.d.
Band 5	.06	.03	.06	.02
Band 6	.52	.68	.72	.85

Table II

Summary of spectral properties of mono-FITC-toxins.

	Absorbance λ Max. nm	ϵ $M^{-1}cm^{-1}$	Quantum Yield	Fluorescence Emission λ Max. (nm)		Fractional Change of Fluorescence (ex: 480 nm) Upon Binding mean ± S.D.
				free	bound	
FITC-lys-35-toxin	494	60,000	0.31	520	519	0.61 ± 0.01
FITC-lys-69-toxin	495	71,000	0.41	520	522	0.74 ± 0.03
FITC-lys-49-toxin	494	72,000	0.38	517	519	0.94 ± 0.01
FITC-lys-23-toxin	494	62,000	0.18	519	519	1.96 ± 0.07

Table III

Summary of FITC-Toxin monoconjugate kinetic rate constants of association to (k_1) and dissociation from (k_{-1}) the membrane-associated AcChR.

Rate constant values represent mean %S.D. of the least squares fits to the left-hand portion of the integrated rate equations for a reversible bimolecular reaction 1) or unimolecular dissociation. Numbers in parentheses are the number of determinations. (* from [4])

	k_1 $M^{-1}s^{-1}$	k_{-1} s^{-1}	k_{-1}/k_1 nM
FITC-lys-35-toxin	$2.5 \pm 0.5 \times 10^4$(15)	$5.4 \pm 3.3 \times 10^{-5}$(3)	2.1
FITC-lys-69-toxin	$3.9 \pm 1.3 \times 10^4$(7)	$0.7 \pm 0.3 \times 10^{-5}$(3)	0.2
FITC-lys-49-toxin	$1.7 \pm 0.8 \times 10^4$(5)	$5.3 \pm 2.3 \times 10^{-5}$(3)	3.2
FITC-lys-23-toxin	$1.5 \pm 0.3 \times 10^4$(12)	$3.5 \pm 1.8 \times 10^{-5}$(3)	2.3
native α-toxin*	50×10^4	1×10^{-5}	0.02

SECTION III

CHARACTERIZATION OF TRITC-LYS-23-TOXIN

Thermolysin Digestion and Peptide Mapping. The reduced and S-carboxymethylated TRITC-α-toxin derivative (1.2 nmol) was dissolved in 250 μL of 0.1 M NH_4HCO_3, 5 mM $CaCl_2$, pH 8.1. Thermolysin (1.1 μg) was added, incubated overnight at 37°C, and the sample evaporated to dryness. The fluorescent product of the digest was resolved with two 80-min passes through a Vydac C_{18} column. Initially the digests were eluted with a TFA-acetonitrile gradient between 0 and 40% acetonitrile. The major peak of fluorescence was rechromatographed on the same column with a linear 80-min acetonitrile gradient, 20 to 35%.

Microsequence Analysis. Microsequence analysis of the fluorescent peptide (60 pmol) was performed on a Applied Biosystems Model 470-A gas-phase microsequencer. Phenylthiohydantoin derivatives were analyzed on-line by reverse-phase, microbore HPLC. Repetitive yields of 69-75% were obtained. Sequencing of the fractions associated with the major fluorescent peptide yielded an unambiguous sequence with a linear log recovery *versus* cycle number plot to be tyr-thr-"blank". This sequence is consistent with the sequence for residues 21-23 (Tyr-Try-Lys-); N^{ϵ}-TRITC-Lys did not produce an identifiable derivative by Edman degradation.

Spectroscopic and Binding Characterization TRITC-Lys 23-Toxin. Based on the absorbance and quantitative amino acid analysis, the extinction coefficient of TRITC-Lys 23-toxin was calculated to be 8.4×10^4 $M^{-1}cm^{-1}$ at 550 nm. The enhancements of fluorescence (EX: 550 nm) associated with binding to the membrane-associated and solubilized AcChR were determined to be 3.1 and 1.8, respectively (data not shown). In the presence of detergent, the association and dissociation rate constants of TRITC-Lys 23-toxin binding to the AcChR were $4.8 \pm 0.3 \times 10^5$ $M^{-1}s^{-1}$ ($n=3$) and $1.7 \pm 0.2 \times 10^{-5}$ s^{-1} ($n=3$), respectively. An example of the association reaction is shown in Fig. 11 along with its fit to an integrated rate expression for a reversible bimolecular reaction (Inset, Fig. 11). Examples of the dissociation kinetics are not shown. These rate constants are similar to the association and dissociation binding rate constants of native α-toxin, 5.0×10^5 $M^{-1}s^{-1}$ and 1×10^{-5} s^{-1}, respectively [57].

Modification of Lys 23 with hydroxysuccinimidylbiotin and fluorescein isothiocyanate has previously been observed to reduce the binding affinity of α-toxin [40,55] which can be interpreted as involvement of Lys 23 in the α-toxin-binding surface. Our iodine-quenching results indicated, however, that Lys 23 is not a part of the binding surface. We thus further investigated the effect of chemical modification of Lys 23 on the ability of α-toxin to bind to the AcChR. Why TRITC modification of Lys 23 does not significantly affect the binding activity, while FITC and N-hydroxysuccinimidylbiotin do, is unclear. The greater positive charge of the TRITC moiety may be a factor. Our results with TRITC-Lys 23-toxin show that the effect of chemical modification of Lys 23 on the binding of the α-toxin to the AcChR is a function of the labeling moiety.

Fig. 11. Association TRITC-Lys 23-toxin (10 nM) with membrane-associated AcChR (20nM in α-toxin sites).

Shown is the time course of total fluorescence upon binding at 20° C in buffer. Inset shows the data plotted with an integrated rate expression for a reversible bimolecular mechanism for >90% of the reaction. Procedures used for data analysis are given elsewhere [55].

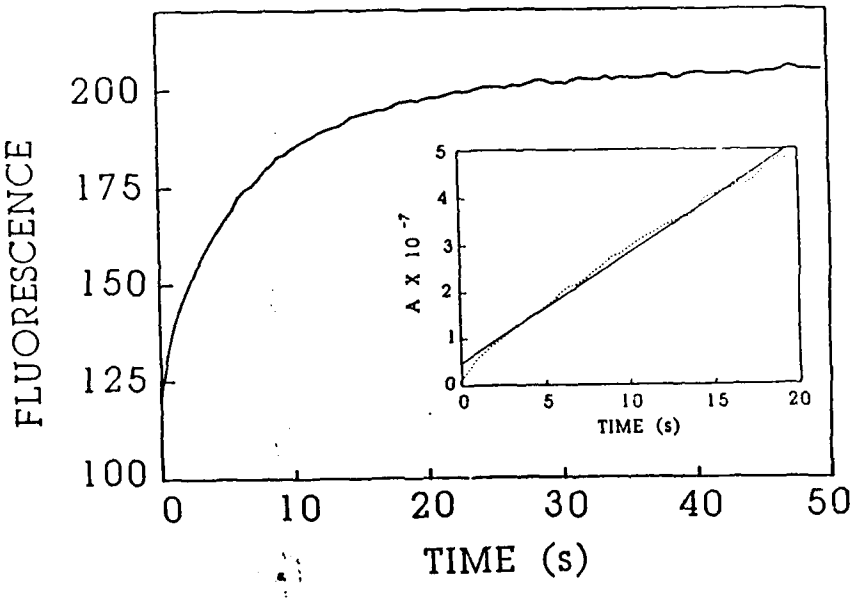

SECTION IV

CHARACTERIZATION OF THE INTERACTION OF ETHIDIUM WITH THE AcChR

Ethidium Inhibits the Binding of [^{3}H]PCP and Is Allosterically Regulated by Occupation of the Agonist Site. To determine directly whether ethidium binds to a noncompetitive inhibitor site on the AcChR, the capacity of ethidium to inhibit [^{3}H]PCP binding was measured. [^{3}H]PCP was selected as a marker of the high-affinity noncompetitive inhibitor site since its stoichiometry of binding has been precisely determined and its interactions with other sites show markedly lower affinities [15]. In agreement with others [15], we found that at concentrations less than 20 μM, [^{3}H]PCP binds to a single class of binding sites on AcChR-enriched membranes either in the presence of carbachol (K_D = 0.4 μM) or in the presence of α-toxin (K_D = 2.0 μM). We also confirmed that the stoichiometry of [^{3}H]PCP binding is approximately one per receptor monomer (0.82 ± 0.17) [50].

Because previous studies have shown that the binding of many noncompetitive inhibitors is allosterically regulated by occupation of the agonist site, we examined competition of ethidium with [^{3}H]PCP in the presence of carbachol and α-toxin (Fig. 12). The large excess of carbachol or stoichiometric excess of α-toxin precludes the possibility of ethidium binding to the agonist site and hence affecting the observed dissociation constants. As shown in Fig. 12, in the presence of carbachol, ethidium competes with [^{3}H]PCP with high affinity (K_D = 0.36 μM) and the data fit a single class of binding sites (solid line). Ethidium in the presence of α-toxin exhibited substantially lower affinity for competing with PCP, with a K_D ~ 1,000 μM. Thus, these data show a pattern of allosteric regulation by the agonist site for ethidium binding typical of many noncompetitive inhibitors, including quaternary amine local anesthetics [50,58].

Allosteric Behavior and Binding of Ethidium to the Agonist Sites. To determine directly the heterotropic effects of ethidium on the agonist sites, a subsaturating concentration of [^{3}H]ACh was used to occupy a fraction of the agonist sites. Under these conditions, conversion of the agonist sites from low affinity (K_D ~1 μM) in the resting state to high affinity (~8 nM) characteristic of the desensitized state, yields a 400% increase in the amount of [^{3}H]ACh bound. As seen in Fig. 13A, increasing concentrations of PCP produce a monophasic increase in the amount of [^{3}H]ACh bound at equilibrium. In contrast, increasing concentrations of ethidium generate a bell-shaped curve; low concentrations (< 10 μM) increase agonist binding while higher concentrations inhibit binding. Similar biphasic curves have been observed with several aromatic amine local anesthetics [21]. This bell-shaped curve may be explained as a combination of two distinct processes: 1) at low concentrations, ethidium binds at the noncompetitive site and its occupation converts the receptor to a state with high affinity for agonists, and 2) at high concentrations, ethidium competes directly at the agonist sites. Consistent with this interpretation, the values of the dissociation constants for PCP and ethidium increasing [^{3}H]ACh binding closely correspond to the K_Ds for these compounds binding to the noncompetitive inhibitor site (Table IV).

To resolve the two putative binding components of the bell-shaped ethidium curve, we directly measured the competition at the agonist sites. In this case, saturating concentrations of [^{3}H]ACh were employed to convert the receptor to the high-affinity, desensitized state; thus, ethidium binding at the noncompetitive inhibitor site should not further enhance binding. Figure 13B shows the concentration dependence of the inhibition of [^{3}H]ACh binding. The competition binding between a saturating concentration of [^{3}H]ACh and ethidium was also examined in the presence of a large excess of PCP (250 μM) in order to block ethidium interaction at the noncompetitive inhibitor site. Similar competition binding isotherms were obtained in the two experiments and dissociation constants of ethidium for the agonist site of 18 ± 0.4 μM in the absence of PCP and 11 ± 2.5 μM

in the presence of PCP were calculated for a single class of binding sites. These results show that the relative affinity of ethidium for the agonist site is 40- to 70-fold lower than the affinity for the noncompetitive inhibitor site in the desensitized state.

Fluorescence Spectra of Ethidium Bound to the Noncompetitive Inhibitor Site. Fluorescence spectra of ethidium were substantially altered upon binding to the noncompetitive inhibitor site and were dependent on the functional state of the receptor. Excitation spectra of ethidium obtained in the presence of 1 mM carbachol showed a large increase in fluorescence intensity upon binding to the receptor relative to ethidium in buffer (Fig. 14A). At the same time, the excitation maximum shifted from 480 nm, characteristic of ethidium in buffer, to ~527 nm. Addition of a large excess of PCP (1 mM) to receptor previously equilibrated with ethidium and carbachol resulted in a large reduction in fluorescence intensity. A similar decrease in intensity was seen with addition of a stoichiometric excess of α-toxin. The excitation spectra in the presence of either α-toxin or PCP showed an excitation maximum at 503 nm, a value intermediate between the maxima observed in the presence of carbachol or buffer alone.

The emission spectra of ethidium bound to AcChR membranes showed parallel changes in fluorescence intensity and concomitant shifts in wavelength maxima. Excitation of ethidium in buffer in the visible band at 480 nm produced a low intensity emission centered at 635 nm (Fig. 14B). Binding of ethidium to the AcChR-enriched membranes in the presence of carbachol resulted in a large enhancement in emission and a blue-shift in the spectrum to 598 nm. Addition of either 1 mM PCP or a 10-fold molar excess of α-toxin resulted in a large decrease in the fluorescence emission and red-shift in the emission maxima to 620 nm. For comparison, emission spectra were also obtained by exciting at 290 nm, where energy transfer from protein tryptophan residues to ethidium should occur in addition to direct excitation (Fig. 14C). As in the case of excitation in the visible band, the emission intensity in the presence of carbachol was greatly enhanced in intensity and exhibited a 35 nm blue shift in the maximum, while in the presence of either PCP or α-toxin, emission was of lower intensity and shifted to the blue by only 15 nm. The greater enhancement in fluorescence emission observed for 290 nm versus 480 nm excitation reflects energy transfer from protein tryptophan residues to ethidium bound at the noncompetitive inhibitor site. Excitation spectra of ethidium show a strong absorption band between 300-355 nm which overlaps tryptophan fluorescence emission. Energy transfer was confirmed by measuring a specific decrease (12%) in the tryptophan fluorescence emission (λ_{max} = 338 nm) from AcChR-enriched membranes in the presence of ethidium (data not shown).

We have defined nonspecific binding in this study with respect to two independent criteria: 1) displacement by saturating concentrations of noncompetitive inhibitor ligand, and 2) by converting the noncompetitive inhibitor site to a state of very low affinity for ethidium with α-toxin. The nonspecific binding that remains under these conditions would be primarily composed of the nonsaturable partitioning of ethidium into the bulk lipid phase of the AcChR-enriched membranes. Part of the nonspecific binding may also include the association of ethidium with the lipid -AcChR interfacial region. Since the ethidium emission spectra obtained in the presence of carbachol are composite spectra composed of specific and nonspecific components, spectral subtraction was carried out to visualize the specific component. As seen in Fig. 14D, difference spectra were generated by subtracting the nonspecific component defined either by excess PCP or by saturating levels of α-toxin. In both cases, the spectral shape and emission maxima of the difference spectra were identical (λ_{max} = 598 nm). The difference emission spectra obtained by excitation at 290 nm or at 480 nm also had similar spectral line shape and emission maxima. Thus, the noncompetitive inhibitor site as identified by spectral criteria is the same when specific binding is defined either with reference to excess noncompetitive inhibitor or by converting the receptor to a low-affinity state by dissociating agonist with α-toxin.

Spectral properties of ethidium bound only to the agonist sites were determined in the presence of saturating concentrations of PCP. Excitation spectra showed a maximum at 504 nm. This value is significantly different from ethidium bound at the noncompetitive inhibitor site, but does not differ appreciably from the maxima for nonspecifically bound ethidium. Emission spectra (λ_{ex} = 290 nm) of ethidium bound at the agonist site exhibited a much smaller increase in fluorescence intensity compared to the noncompetitive inhibitor site. Excitation in the UV and visible both produced similar emission maxima that did not differ greatly from maxima obtained for nonspecific binding in the presence of either excess agonist or α-toxin, but difference spectra showed a maxima at 614 nm. Thus, the fluorescence intensities, as well as excitation and emission maxima are significantly different for ethidium bound to the noncompetitive inhibitor and agonist binding sites.

Fluorescence Titrations of Ethidium Association with AcChR-Enriched Membranes. To characterize the interactions of ethidium with the noncompetitive inhibitor site, fluorescence titrations were performed using AcChR-membranes in the presence of 0.5 mM carbachol. As seen in Fig. 15A, the total binding of ethidium could be resolved into a hyperbolic saturable binding isotherm superimposed on a linear, nonspecific component. The nonspecific fluorescence component was identified by titrations either in the presence of excess PCP or a 10-fold excess of α-toxin, and found to be identical. Subtraction of the linear component defined by either excess competing ligand or by maintaining the binding site in a low-affinity conformation yielded equivalent saturable binding components. A Scatchard plot of these data shown in Fig. 15B indicates that ethidium binds to a single class of non-interacting sites distinct from the agonist binding sites with a dissociation constant equal to 0.25 μM. The dissociation constant determined by fluorescence was in reasonable agreement with the corresponding value of 0.36 μM determined by competition with [^{3}H]PCP.

The stoichiometry of the high-affinity ethidium binding sites was determined by fluorescence titration under conditions where the number of ethidium binding sites was in large excess over the K_D for ethidium (Fig. 15C). In this experiment, substantial light scattering due to the membrane fragments limited the concentration of sites that could be used for titration. Extrapolation of the linear increase in specific fluorescence intensity which reflects ethidium binding stoichiometrically, to the level reached at saturation yielded an estimate of 0.90 ± 0.1 μM for the ethidium site concentration. Since the concentration of α-toxin sites was 2.0 μM, the number of ethidium sites is equal to half the number of α-toxin sites.

Dissociation of Bound Ethidium by Noncompetitive Inhibitor Ligands. Figure 16A and B show back titrations of ethidium fluorescence by well-characterized noncompetitive inhibitors when the agonist sites are saturated with carbachol. As seen in Fig. 16A, competitive dissociation of ethidium by PCP was directly monitored by a decrease in ethidium fluorescence at 593 nm upon excitation at 500 nm and yielded an apparent IC_{50} of 1.5 μM. The fluorescence intensity reached at saturating concentrations of PCP was equal to that obtained in the presence of excess α-toxin. Similar dissociation curves were obtained using H8-HTX and dibucaine in back-titrations, and the fluorescence intensities obtained at saturating concentrations of all three competing ligands were the same. The fluorescence back titration data for PCP, H8-HTX and dibucaine were analyzed (Fig. 16B). Table IV shows that the dissociation constants calculated for the competing ligands were found to closely agree with values determined by direct radioligand binding (for [^{3}H]PCP) and by competition binding with [^{3}H]PCP (H8-HTX and dibucaine). Cohen and coworkers (1985) have also found that ethidium displaced [^{3}H]HTX in the presence carbachol with a IC_{50} of ~1 μM. The competitive titration curves exhibit slopes in the logarithmic plots that are not significantly different from unity (Table IV). Because the slopes are unity, the competing ligands bind to a homogeneous class of independent sites in causing ethidium dissociation.

Effect of Ligand Occupation of the Agonist/Antagonist Site on Ethidium Fluorescence. An additional characteristic of the ethidium fluorescence signal from the noncompetitive inhibitor site should be the allosteric regulation by agonists, as previously demonstrated by competition binding with [^{3}H]PCP (Fig. 12). To determine the effect of agonists on ethidium fluorescence originating from the noncompetitive inhibitor site, titrations with carbachol were performed (Fig. 17). The specific fluorescence change was calculated by correcting for nonspecific changes that occurred in the presence of a fivefold excess of α-toxin. In this experiment, the concentration of agonist sites was approximately equal to the K_D of carbachol. The solid line through the data is a theoretical curve calculated from the law of mass action for a carbachol dissociation constant of 1.4 μM assuming an equivalence of carbachol and α-toxin sites. The apparent dissociation constant obtained from this curve is similar to the K_D obtained from the inhibition of the initial rate of α-toxin binding by carbachol after equilibrium exposure [59]. A Hill plot of carbachol titration data indicated a Hill coefficient significantly greater than unity ($n = 1.27 \pm 0.10$). This suggests that modest positive cooperativity between subunits involved in the association of carbachol is monitored by ethidium at the noncompetitive inhibitor site.

Fluorescence Lifetime Analysis. The fluorescence lifetime of ethidium bound to the noncompetitive inhibitor site was examined in order to clarify the mechanism responsible for the increase in fluorescence intensity that occurs upon carbachol binding. UV excitation was employed to enhance the contribution of the specifically bound ethidium fluorescence. As seen in Fig. 18C, the fluorescence decay rate for ethidium in buffer followed a single exponential function. The lifetime was calculated to be 1.7 ns, in good agreement with previously determined values [60]. The corresponding fluorescence decay rates of AcChR-membranes containing ethidium bound at the noncompetitive inhibitor site (Fig. 18A) and nonspecifically bound (Fig. 18B) showed dramatic increases in fluorescence lifetimes (Table V). For ethidium bound to the AcChR at the noncompetitive inhibitor site, only a single exponential was required to fit the decay, yielding a lifetime of 22.2 ns. However, the fluorescence decay curve of ethidium under conditions of nonspecific binding did not follow a single exponential decay behavior, but was described by an equation containing two exponential terms. The fluorescence decay was characterized by a short lifetime component ($\tau_1 = 1.8$ ns) and a longer lifetime component ($\tau_2 = 22.1$ ns) with a ratio of amplitudes (a_1/a_2) of 7.5. The short lifetime was nearly identical to that observed for ethidium only in buffer, which indicated that PCP displaced ethidium from its binding site into the aqueous phase. The preexponential factors (a_1 and a_2) give the fractional population of each component, which in this case correspond to free (a_1) and nonspecifically bound (a_2) ethidium. AcChR and ethidium in the presence of excess α-toxin also showed two-exponential decay behavior with nearly identical lifetimes and ratio of preexponential factors. Titration of AcChR with ethidium to achieve fractional occupation of the noncompetitive inhibitor site showed a rough correspondence between the decrease in the a_1/a_2 ratio and site occupation (data not shown). The assignment of free, specifically bound, and nonspecifically bound lifetime components is supported by lifetime analysis of data obtained from the above samples by excitation in the visible band. In contrast to the data obtained by UV excitation, the fluorescence decay for ethidium bound at the noncompetitive inhibitor site clearly required a two-exponential fit. A short lifetime component ($\tau_1 = 2.3$ ns) corresponding to ethidium in buffer was observed in addition to the longer lifetime component ($\tau_2 = 21.9$ ns) characteristic of specifically bound ethidium ($a_1/a_2 = 2.5$). This long lifetime component corresponded to the same lifetime observed with UV excitation. Addition of 1 mM PCP greatly increased the ratio of the free-to-bound amplitudes ($a_1/a_2 = 18.5$) while not changing the two lifetime values. Thus, the single exponential decay found for specifically bound ethidium with UV excitation can be attributed to the selective excitation of ethidium bound to the noncompetitive inhibitor site that is due to energy transfer from protein tryptophan residues.

Steady-State Polarization of Ethidium Fluorescence. The mobility of ethidium bound to the noncompetitive inhibitor site was determined by steady-state fluorescence polarization measurements. Ethidium was excited in the main visible transitions located at 480 nm in buffer and at 520 nm when bound to the noncompetitive binding site. As seen in Table VI, ethidium polarization in buffer is negligible as expected for a small fluorophore undergoing rapid isotropic rotation. Ethidium (1.0 μM) bound to AcChR (1.0 μM α-toxin sites) in the presence of saturating concentrations of carbachol shows an extremely high polarization value, P = 0.4 ± .01. In the case of ethidium binding to the AcChR in the presence carbachol, the large enhancement in fluorescence upon binding weights the steady-state polarization measurement in favor of the specifically bound ligand population. A Perrin plot of ethidium in buffer was used to determine a limiting polarization (P_o) value of 0.40 (data not shown). Ethidium bound to the noncompetitive inhibitor site approaches the maximal limiting polarization value, indicating its strong immobilization. Addition of a large excess of PCP to the specifically bound ethidium AcChR-carbachol complex resulted in a substantial decrease in polarization to 0.22 ± 0.01. Moreover, prior incubation of AcChR with excess α-toxin also significantly decreased the ethidium polarization to 0.27 ± 0.01. The similar reductions in polarization for ethidium in the absence of specific binding partly reflect the displacement of ethidium from its binding site and transfer to the aqueous phase. The intermediate polarization value also indicates that the remaining nonspecifically bound ethidium is also substantially immobilized.

Summary. Our study demonstrates that ethidium can be utilized as a specific fluorescence probe of the noncompetitive inhibitor site on the AcChR from *Torpedo californica*. Both radioligand competition binding and direct fluorescence titrations show that ethidium binds to a single site, distinct from the agonist binding sites, whose affinity is allosterically regulated by agonist binding. Binding of ethidium to the noncompetitive inhibitor site also converts the receptor to a state exhibiting increased agonist affinity. The noncompetitive inhibitor ligands, PCP, H8-HTX, and dibucaine, were found to completely displace specifically bound ethidium, indicating a common binding site for all four ligands.

Table IV

Equilibrium Dissociation Constants for Noncompetitive Inhibitor Ligands Binding to the *Torpedo* AcChR.

Ligand	K_D[a] (μM)	$K^b_{R'A}$ (μM)	$K^c_{R,A}$ (μM)	$K_{R,A}/K_{R'A}$ (μM)	K^D_{des} (μM)	n_H[a]
Ethidium	0.25	0.36	~1,000	~2778	0.72	1.23
PCP	0.40	0.40	2.0	5.0	3.5	0.93
H8-HTX	0.044	0.031	-	-	-	0.98
Dibucaine	1.00	1.7	57.1	34.6	-	1.05

[a]Determined by fluorescence back titration of ethidium with competing ligands in the presence of 1 mM carbachol and using K_D = 0.25 μM for ethidium. [b]Determined by competition binding with [^{3}H]PCP in the presence of 1 mM carbachol. [c]Determined by competition binding with [^{3}H]PCP in the presence of a 10-fold excess of α-toxin. [d]Determined by the increase in [^{3}H]ACh binding.

Table V

Fluorescence Spectral Properties of Ethidium Bound to the Noncompetitive Inhibitor and Agonist Binding Sites.

Ligands[a]	Excitation maxima[c] (nm)	Emission maxima[d] (nm)	K_D (μM)
Ethidium in buffer	480[a]	635[a]	---
AcChR + CARB + ethidium	527[a,c]	598[a,c]	0.36
AcChR + ethidium + PCP	504[b,c]	614[b,c]	11.0
AcChR + CARB + ethid.+PCP	503[b]	620a	—
AcChR + α-toxin+ethid.	503[b]	620[a]	—

[a]Concentrations for the samples were: AcChR, 1.0 μM α-toxin sites; ethidium, 1.0 μM; carbachol, 0.5 mM; PCP, 1.0 mM; α-toxin, 10.0 μM. [b]Concentrations for the samples were: AcChR, 1.0 μM α-toxin sites; ethidium 10.0 μM; PCP, 200 μM. [c]Wavelength maxima obtained from difference spectra.

Table VI

Fluorescence Lifetimes, Amplitudes, and Polarization for Ethidium Bound to AcChR-Enriched Membranes[b]

Ligands[a]	a_1	τ_1(ns)	a_2	τ_2(ns)	a_1/a_2	χ^2/N	P[c]
Ethidium in buffer	-	1.7	-	-	-	6.5	.02
AcChR + CARB + ethidium	-	22.2	-	-	-	2.0	.41
AcChR + CARB + ethidium+PCP	.88	1.4	.12	21.5	7.5	8.6	.22
AcChR + α-toxin + ethidium	.88	1.5	.12	22.1	7.3	5.5	.27
AcChR + ethidium	.75	2.0	.25	20.6	3.0	1.8	-

[a]Concentrations for the above samples were: AcChR, 1.0 μM α-toxin sites; ethidium, 1.0 μM; carbachol, 0.5 mM; PCP, 1.0 mM; α-toxin, 5.0 μM. [b]Excitation and emission bands were selected with a Corning 7-54 and 3-70 filter, respectively. [c]Polarization (P).

Fig. 12. Inhibition of the binding of [^{3}H]PCP by ethidium and its allosteric regulation by agonist occupation.

Acetylcholine receptor-enriched membranes (1.0 μM α-toxin sites) and 1.0 μM [^{3}H]PCP were incubated with either 1.0 mM carbachol (■) or 10 μM α-toxin (▲) and ethidium at the specified concentrations. Specifically bound [^{3}H]PCP was determined by subtracting the binding in the presence of 1.0 mM nonradioactive PCP from the total binding. The two competition curves have been normalized to 100% binding to facilitate comparison of ethidium affinities in the resting and desensitized receptor states. The solid lines through the data were fit by nonlinear least squares analysis assuming a single class of binding sites.

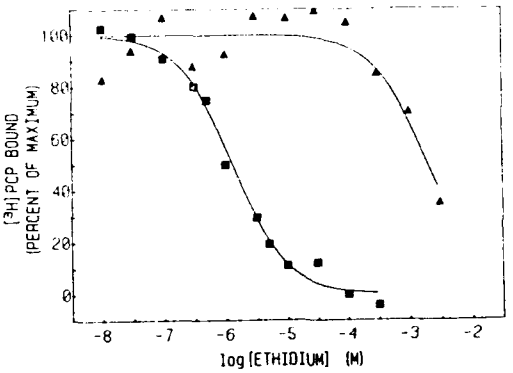

Fig. 13. The influence of ethidium and PCP on the binding of [^{3}H]acetylcholine to AcChR-enriched membranes.

(A) Effects determined by fractional occupation of agonist binding sites in the absence of added noncompetitive ligand. AcChR-membranes were pretreated with 0.1 mM DFP for 1 hr. The membranes (25 nM α-toxin sites) were incubated with 25 nM [^{3}H]ACh at the specified concentrations of PCP (■) and ethidium (O). Free and bound [^{3}H]ACh were separated by filtration as described under Materials and Methods.

(B) Inhibition of [^{3}H]ACh binding by ethidium. DFP-pretreated AcChR-enriched membranes (100 nM α-toxin sites) were incubated with 100 nM [^{3}H]ACh either in the absence (●) or presence of 250 μM PCP (■) at the specified concentrations.

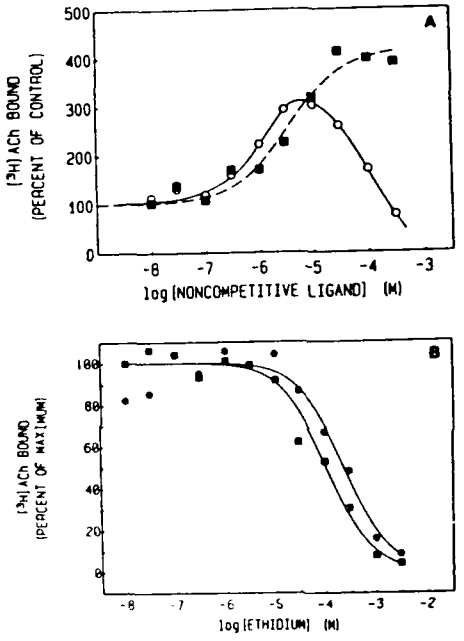

Fig. 14. Effect of agonists, antagonists and noncompetitive inhibitors on the fluorescence spectra of ethidium bound to AcChR-enriched membranes.

(A) Corrected fluorescence excitation spectra of: 1) AcChR-membranes (1.0 μM α-toxin sites) in the presence of 1 mM carbachol and 1.0 μM ethidium, 2) AcChR membranes (1.0 μM α-toxin sites), preincubated with 10.0 μM α-toxin, and 1.0 μM ethidium, 3) AcChR membranes (1.0 μM α-toxin sites), 1 mM carbachol; 1.0 μM ethidium, and 200 μM PCP. All solutions were in 100 mM NaCl, 10 mM $NaPO_4$, pH 7.4. Emission was measured at 593 nm, 4) 1.0 μM ethidium in buffer, 5) 10 μM ethidium, AcChR-membrane (5.0 μM in α-toxin sites) and PCP (200 μM).

(B) Corrected fluorescence emission spectra of samples 1, 2, 3, 4 and 5 as described above in (A). Excitation wavelength was 480 nm.

(C) Corrected fluorescence emission spectra of samples 1, 2, 3, 4 and 5 as described above in (A). Fluorescence was excited at 290 nm, allowing energy transfer from AcChR tryptophan residues to ethidium.

(D) Fluorescence emission difference spectra of ethidium bound to the noncompetitive inhibitor site. Difference spectra obtained using excess PCP to define nonspecific binding and (1) exciting at 480 nm or (2) exciting at 290 nm. Difference spectra obtained using α-toxin to define nonspecific binding, and (3) exciting at 480 nm, or (4) exciting at 290 nm. Difference spectra of ethidium bound to the agonist site were obtained by subtracting the spectrum of (5) in the presence of 10.0 μM α-toxin. All spectra have been normalized with respect to their maximum intensity for comparison of emission maxima and spectral shape.

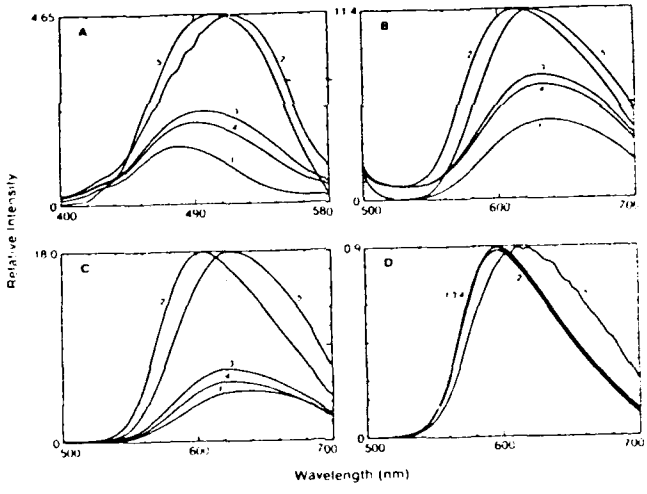

Fig. 15. (A) Fluorescence titration of AcChR-enriched membranes with ethidium in the presence of carbachol.

AcChR-membranes (0.2 μM α-toxin sites) were equilibrated with 0.5 mM carbachol. Titrations were carried out in 100 mM NaCl, 10 mM $NaPO_4$, pH 7.4 at 25°C. (O-O), AcChR and carbachol, (▵-▵) AcChR, carbachol, and 1 mM PCP, (▲-▲) AcChR, carbachol and 10.0 μM α-toxin.

(B) Scatchard plot of the fluorescence titration of AcChR with ethidium in the presence of carbachol. The specific binding of ethidium was calculated from the data in (A) was found to be identical using either the nonspecific binding determined in the presence of 1 mM or 10 μM PCP or 10 μM α-toxin. Calculations are based upon saturation of binding sites resulting in 1 mole of ethidium bound per 2 moles α-toxin binding sites.

(C) Stoichiometry determined from the fluorescence titration of AcChR-enriched membranes in the presence of carbachol with ethidium. AcChR-enriched membranes (2.0 μM α-toxin sites) were equilibrated with 0.5 mM carbachol. Other experimental conditions as described in (A). (O-O) total fluorescence, (▵-▵) nonspecific binding determined in the presence of 1 mM PCP, (●-●) specific fluorescence changes. The solid lines extrapolated from the stoichiometric region of binding and the level achieved at saturation intersect at 1.0 μM ethidium, indicating 1 mole of ethidium binding sites per 2 moles α-toxin binding sites.

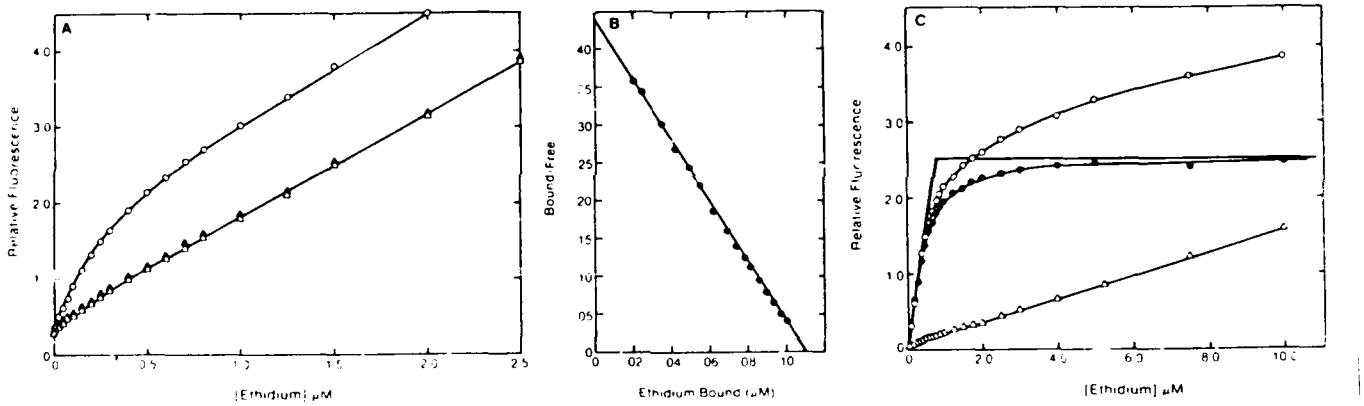

Fig. 16. (A) Dissociation of the ethidium-AcChR complex in the presence of carbachol by PCP. Incremental additions of PCP were made to a solution containing AcChR-membranes (1.0 μM α-toxin sites), 1.0 μM ethidium, and 0.5 mM carbachol. Titration profile derived from measurement of ethidium fluorescence (λ_{ex} = 500 nm, λ_{em} = 593 nm).

(B) Hill plots of the competitive dissociation of ethidium from AcChR-membranes in the presence of carbachol by noncompetitive inhibitor site ligands. Experimental conditions are as in (A), above. Data are plotted logarithmically where [C] and [E] are concentrations of the competing ligand and ethidium, respectively. f_E denotes the initial fluorescence in the absence of competing ligands, f_c denotes the fluorescence when ethidium is completely displaced from the AcChR, and f denotes the fluorescence observed at any given concentration of competing ligand during the titration (O-O) PCP, (■-■) H8-HTX, (●-●) dibucaine.

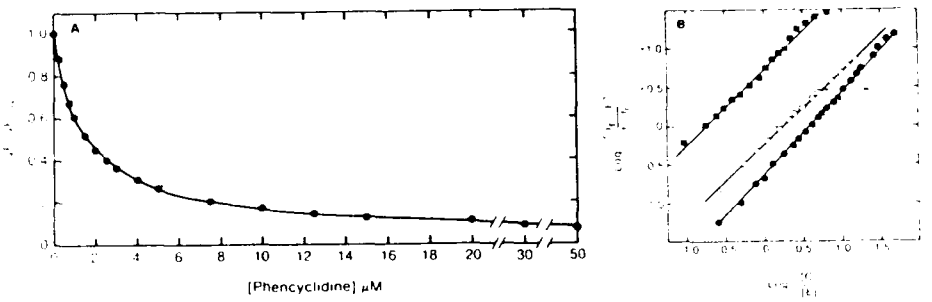

Fig. 17. The effect of association of carbachol on the binding of ethidium to AcChR-enriched membranes.

Torpedo AcChR membranes (1.0 μM α-toxin sites) were equilibrated with 1.0 μM ethidium prior to incremental addition of carbachol. The titration profile was obtained by measurement of ethidium fluorescence (λ_{ex} = 290 nm, λ_{em} = 594 nm). Nonspecific changes in fluorescence were measured in an equivalent sample containing either 0.5 mM PCP or 10.0 μM α-toxin. The solid line through the data is a theoretical curve calculated from the law of mass action and assuming 1.0 μM carbachol binding sites.

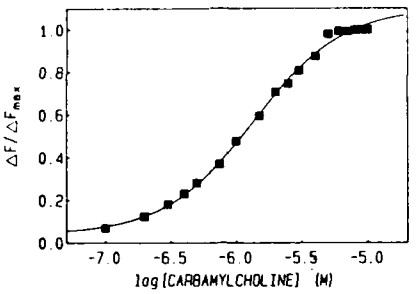

Fig. 18. Fluorescence lifetime measurements of ethidium bound to AcChR-enriched membranes.

The fluorescence lifetime of ethidium was measured using excitation in the UV absorption band in the following solutions: A) 1.0 μM α-toxin sites AcChR enriched membranes, 0.5 mM carbachol and 1.0 μM ethidium; (B) 1.0 μM α-toxin sites AcChR enriched membranes, 0.5 mM carbachol and 1.0 mM PCP; (C) 10.0 μM ethidium in 100 mM NaCl, 10 mM $NaPO_4$, pH 7.4.

Each panel shows the lamp pulse (dashed line), the raw data (dotted line) and the computer-calculated decay curve (solid line) obtained from deconvolution of the experimental decay with the lamp pulse by the method of moments. The residual analysis (χ^2/N) for deviation of the calculated curve from the data is shown for sample A.

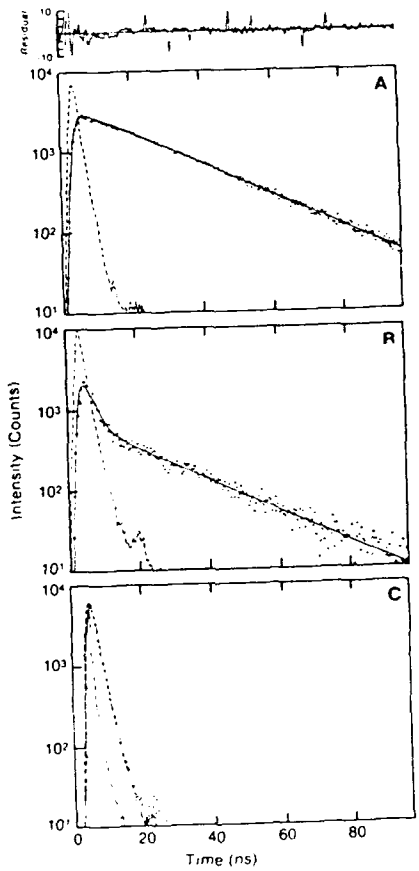

SECTION V

CHARACTERIZATION OF THE INTERACTION OF DECIDIUM WITH THE AcChR

Decidium inhibition of initial rate of [^{125}I]-labeled α-toxin binding and agonist-stimulated $^{22}Na^+$ permeability. Decidium inhibition of the initial rate of [^{125}I]-labeled α-toxin binding to both *Torpedo* AcChR-enriched membrane fragments and intact BC3H-1 cells was examined after instantaneous and prolonged (30 min) exposure to decidium. Decidium inhibits α-toxin binding to AcChR in *Torpedo* membranes (Fig. 19A) and in intact BC3H-1 cells (Fig. 19B). In each case the binding profiles exhibit Hill coefficients (n_H) less than unity. Decidium also inhibits $^{22}Na^+$ influx stimulated by carbachol in BC3H-1 cells (Fig. 19C) at slightly lower concentrations but with a somewhat steeper profile (Table VII). As seen in *Torpedo* [59,61] and in BC3H-1 cells [62], the Hill slope of less than unity for occupation suggests nonequivalence of decidium K_D's for the two agonist sites on the receptor. The steeper slope and the dependence on lower antagonist concentrations for blockade of the functional response shows that occupation of only one of the two sites is adequate to achieve functional antagonism, as documented for the classical antagonists [62]. In control experiments, decidium alone did not increase $^{22}Na^+$ permeability over basal values, indicating that it has no partial agonist activity (data not shown).

The decidium protection constants decreased 2-4 fold when decidium was added 30 min prior instead of simultaneously with radiolabeled α-toxin addition (Fig. 19, Table VII). This observation suggests that decidium possesses a limited capacity to convert AcChR to a state which displays increased affinity for decidium. Such a conversion in AcChR state might occur by decidium acting at the agonist site as a metaphilic antagonist [63, 64] or by acting at an allosteric site as a noncompetitive, heterotropic inhibitor. In both cases, a slow conversion to a state possessing a higher affinity for decidium is predicted.

Decidium Inhibition of Agonist Activation of AcChR Permeability Response. To examine the mechanism of decidium inhibition, the concentration dependence for carbachol activation of $^{22}Na^+$ permeability was measured in BC3H-1 cells in the presence of decidium. For comparison, a metaphilic antagonist,dinaphthyldecamethonium [63, 64], and a classical antagonist,d-tubocurarine were also examined. Increasing decidium concentrations progressively shift the carbachol concentration-response curve to higher agonist concentrations as well as reduce the maximal response obtained at saturation (Fig 20A). This behavior indicates both competitive and noncompetitive components of decidium inhibition are present. Like decidium, dinaphthyldecamethonium displays apparent noncompetitive inhibition, consistent with conversion of AcChR to a desensitized state incapable of channel opening (Fig. 20B). d-Tubocurarine, by contrast, shifts the curve to higher agonist concentrations without altering the maximal permeability response (Fig. 20C).

Decidium Enhancement of Agonist Competition with α-Toxin Binding. The previous data do not distinguish whether decidium converts AcChR to a state of increased agonist affinity and decreased functional responsiveness by association at the agonist site or at heterotropic, allosteric site(s). If decidium action was exerted solely at the agonist site, then decidium enhancement of the apparent agonist affinity should occur over the same concentration range as decidium competition with [^{125}I]-labeled α-toxin binding. Alternatively, if decidium converts the AcChR to a state of increased agonist affinity by an allosteric mechanism as has been demonstrated for the noncompetitive inhibitors [4, 65-67], we should observe a separation between the concentration dependence for direct decidium competition and allosteric enhancement of agonist competition with α-toxin binding. To address this question, we examined the concentration dependence for decidium augmentation of the competition of agonist with the initial rate of [^{125}I]-labeled α-toxin binding, and

these results were compared to the concentration dependence for decidium competition of the initial rate of[^{125}I]-labeled α-toxin binding. Data on *Torpedo* membranes (Fig. 21A) and BC3H-1 cells (Fig. 21B) show identical decidium concentration dependence for inhibition of α-toxin binding and for augmentation of the competition of carbachol with α-toxin binding. For comparison, Fig. 21C shows the corresponding result obtained with the local anesthetic meproadifen in *Torpedo* membranes. Here, meproadifen enhances carbachol competition with α-toxin binding at far lower concentrations than those required for inhibition of α-toxin binding.

Decidium Modulation of [^{3}H]PCP Binding. [^{3}H]PCP has been shown previously to bind selectively to a site on the receptor which is noncompetitive with and allosterically coupled to agonist binding [50, 68]. Prolonged occupancy by agonists and certain antagonists converts the receptor to a desensitized state exhibiting increased agonist affinity as well as increased affinity for noncompetitive inhibitors such as PCP. Occupancy of the agonist site by α-toxin prevents the conversion of the receptor to the desensitized state. Conversely, occupancy of the noncompetitive inhibitor site by PCP converts the receptor to a state exhibiting increased affinity for certain agonists [69]. We therefore examined the influence of decidium on [^{3}H]PCP binding to the *Torpedo* AcChR in the absence and presence of excess carbachol or α-toxin (Fig. 22). A subsaturating concentration of[^{3}H]PCP was used in order to monitor both increases or decreases in the capacity of [^{3}H]PCP to bind to the AcChR.

When the agonist sites are occupied with saturating concentrations of carbachol or α-toxin, increasing concentrations of decidium displace [^{3}H]PCP,consistent with direct action of decidium at the noncompetitive inhibitor site in its high- and low- affinity states, respectively. As expected, carbachol alone enhances the fraction of bound [^{3}H]PCP. Using previously determined values for the K_Ds of PCP toward the desensitized and resting receptor states, the K_Ds of decidium toward the site in these two states were calculated to be 1.2 μM and 29 μM, respectively.

In the absence of either carbachol or α-toxin, decidium exhibits biphasic effects on [^{3}H]PCP binding (Fig. 22). Low concentrations of decidium increase [^{3}H]PCP binding to the level observed in the presence of carbachol, suggesting that decidium interaction at the agonist site converts the receptor to a state exhibiting increased [^{3}H]PCP binding. At higher concentrations decidium inhibits [^{3}H]PCP binding, indicating decidium directly competes with the PCP binding site.

Spectroscopic Characterization of decidium-AcChR Complexes. Excitation and emission fluorescence spectra of decidium complexed with the agonist and high-affinity noncompetitive inhibitor sites were obtained either in the presence of excess PCP, to block the noncompetitive inhibitor site, or excess carbachol, to block the agonist site. Contributions to the spectra arising from free ligand and light scatter were subtracted to yield the difference spectra. The corrected excitation maximum of decidium complexed with the agonist site appears at 490 nm, while the excitation maximum of decidium at the noncompetitive inhibitor site appears at 530 nm (Fig. 23A). The fluorescence emission maximum of decidium complexed to the agonist or the high-affinity noncompetitive inhibitor sites appear between 605 and 610 nm (Fig. 23B). The apparent quantum yield of decidium increases about two-fold upon binding to either the agonist or the noncompetitive inhibitor sites.

Fluorescence Titrations. Equilibrium binding parameters for decidium association at the agonist sites were determined by fluorescence titrations (Fig. 24). Excitation at 290 nm was used to maximize the signal from the bound fluorophore. The spectral overlap between receptor tryptophanyl emission and decidium absorbance in the 340 nm band results in substantial enhancement of the bound decidium signal relative to 480 nm excitation. All samples contained 100 μM PCP to prevent decidium binding to the noncompetitive inhibitor site. Fig. 24B shows the specific fluorescence from decidium bound to the agonist sites,where nonspecific binding was defined using excess cobra α-toxin. In four replicate titrations we obtained composite values of K_D

= 0.57±0.34 μM and n_H =0.89±0.19.

The observation of a Hill coefficient less than unity suggested nonequivalence of decidium dissociation constants at the agonist sites. We also carried out displacement titrations of decidium by the agonist carbachol, which displays a unitary Hill coefficient for binding [57] (Fig. 25). At saturation, carbachol reduces decidium fluorescence to a similar extent as excess α-toxin. Hill analysis of the data (Fig. 25B) reveal n_H = 0.85. The observation of Hill coefficients less than unity for displacement of decidium further suggests some nonequivalence for the interaction of decidium at the agonist sites, in accord with the pharmacological studies. Analogous results were obtained by competition with the partial agonist decamethonium (data not shown).

Energy Transfer between FITC-toxin and Decidium. To examine the distance between the two agonist sites on the individual receptor molecules, we assessed dipolar fluorescence energy transfer between FITC-toxin and decidium bound to the agonist sites on the receptor. Doubly-liganded receptors were prepared to achieve the fractional occupation. Saturating concentrations of PCP were added to prevent decidium binding to the noncompetitive inhibitor site. The spectral overlap integral between FITC emission and decidium excitation, J, was calculated to be 2.49 x 10^{-14} cm^3M^{-1} (cf. Fig. 22 and data not shown). Assuming a refractive index of 1.4 and an orientation factor (κ^2) of 0.67, R_o was calculated to be 30 Å.

Various factors render quantification of steady state energy transfer between FITC-toxin and decidium bound to the AcChR difficult. These factors include the significant overlap of decidium and FITC emission spectra, and the inner filter effects of decidium at the FITC absorption maxima. Since fluorescence lifetimes are unaffected by inner filter effects and since an appropriate combination of interference filters could be chosen which reduces the contribution of decidium fluorescence to less than five percent of the FITC fluorescence signal, we have chosen to determine energy transfer as the extent of reduction of donor FITC fluorescence lifetime in the presence of the acceptor decidium. The results of studies on membrane-associated and detergent solubilized receptor preparations are presented in Fig. 26 and Table VIII. In the absence of added decidium and with 15% occupancy by FITC-toxin, the exponential decay of FITC-toxin fluorescence was satisfactorily described by a single fluorescence lifetime (τ=3.9 ns). When decidium was added to saturate the remaining agonist sites, a sixteen percent decrease was observed in the fluorescence lifetime of FITC-toxin bound to the membrane-associated AcChR (Fig. 26A). This quenching was not altered by the further addition of native α-toxin (Fig. 26B) and was abolished by solubilizing the receptor with cholate (Figs. 26C and D). Taken together, the reduction in FITC-toxin fluorescence lifetime does not stem from decidium at the agonist site but reflects energy transfer between FITC-toxin bound to the agonist site and decidium partitioned nonspecifically into the lipid bilayer. If we assume a detection limit of five percent transfer between agonist sites, then the predicted minimum separation between fluorophores at the agonist sites of 1.63 x R_o, or 49 Å. Hence, the greater than 49 Å separation between the agonist sites is too distant to account for the reduction in lifetime of FITC-labeled toxin in the presence of decidium. The minimal but measurable excitation transfer efficiency indicates that at high concentrations decidium can partition into the membrane.

Fig. 19. Decidium inhibition of initial rates of cobra [^{125}I]-labeled α-toxin and carbachol-stimulated $^{22}Na^+$ influx in *Torpedo* membranes and BC3H-1 cells.

Initial rates of [^{125}I]-labeled α-toxin binding to AcChR in (A) *Torpedo* membrane fragments or (B) monolayer BC3H-1 cultures were measured in the presence of the indicated decidium concentrations. Data were normalized to the rate of α-toxin binding in the absence of decidium. Initial rates of carbachol-stimulated $^{22}Na^+$ influx were measured in BC3H-1 cells (C) in the presence of 60 μM carbachol plus the indicated decidium concentrations. Experimental determinations were made in duplicate. Filled circles (●) --equilibrium exposure (30 min) to buffer containing the indicated decidium concentrations followed by initial rate measurements of either [^{125}I]labeled-α-toxin or carbachol-stimulated $^{22}Na^+$ influx in the presence of the indicated decidium concentrations. Open circles (○)--equilibrium exposure to buffer alone (instantaneous decidium exposure) followed by initial rate measurements in the presence of the indicated decidium concentrations. The solid lines represent best nonlinear fits to the Hill equation.

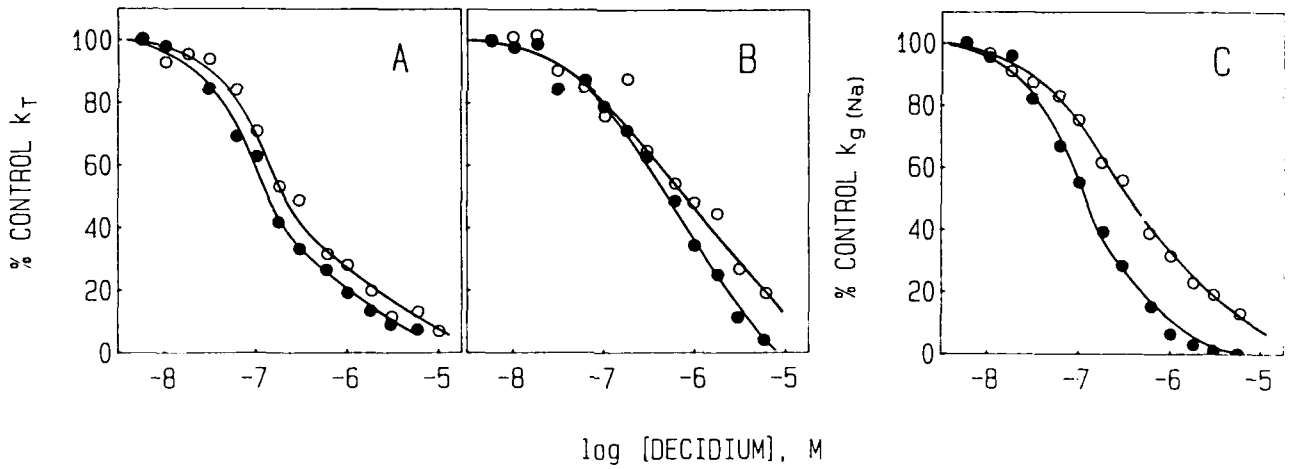

Fig. 20. Antagonist inhibition of concentration-dependent carbachol activation of receptor permeability response in BC3H-1 cells.

$^{22}Na^+$ permeability elicited by the specified concentrations of carbachol plus antagonist over a 20 s interval was measured in sets of culture dishes. Results are expressed as percent of the maximum rate in the absence of antagonist.

(A) Decidium: ■-■, no added decidium; ●-●, 10^{-7} M; ▲-▲, 3 x 10^{-7} M; O-O, 10^{-6} M; □-□, 3x 10^{-6} M. (B) Dinaphthyldecamethonium: ■-■, no added dinaphthyldecamethonium; ●-●, 6 x 10^{-7} M; ▲-▲, 3 x 10^{-6} M; O-O 10^{-5} M. (C) d-Tubocurarine: ■-■, no added d-tubocurarine; ●-●, 3 x 10^{-7} M; ▲-▲, 10^{-6} M; O-O, 6 x 10^{-6} M.

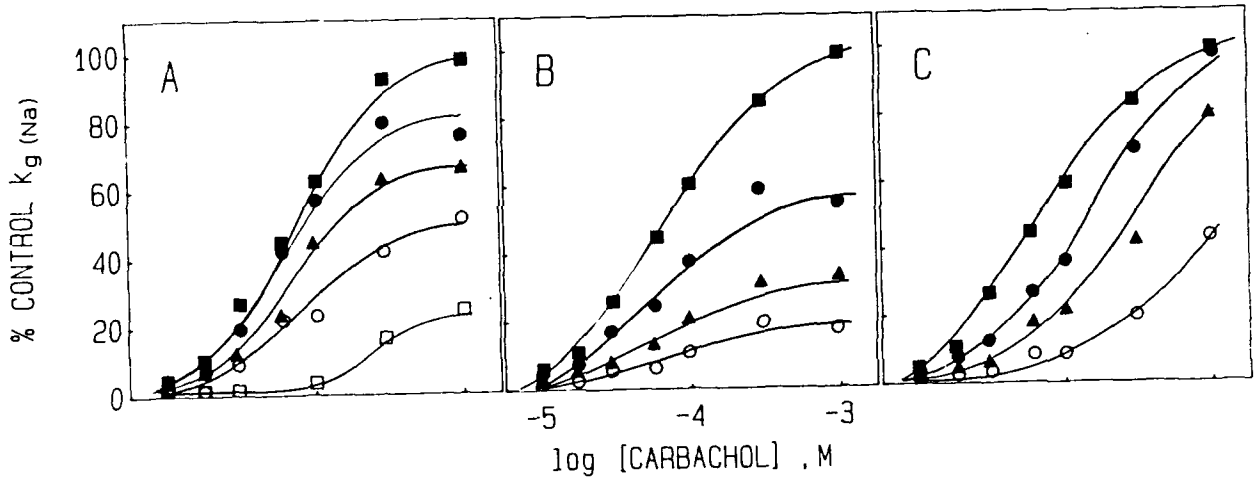

Fig. 21. Decidium and meproadifen enhancement of carbachol competition with the initial rate of [^{125}I]labeled α-toxin binding to AcChR in *Torpedo* membranes and BC3H-1 cells.

Decidium and meproadifen in the specified concentrations were added 30 min before initiating the toxin-binding reaction. Carbachol was added either 10 s or 30 min before addition of α-toxin. Initial rates of toxin binding were measured over 40 s and expressed as a percent of the rate observed in the absence of added effector. ○-○, rate of binding measured with 10 s of prior exposure to agonist; ●-●, rate of binding with 30 min of prior exposure to agonist; ■-■, rate of binding with exposure only to decidium or meproadifen. (A) Decidium, *Torpedo* membranes. The test carbachol was 1 μM. (B) Decidium, BC3H-1 cells. The test carbachol was 30 μM. (C) Meproadifen, *Torpedo* membranes. The test carbachol concentration was 1 μM. Asterisk indicates overlapping data points.

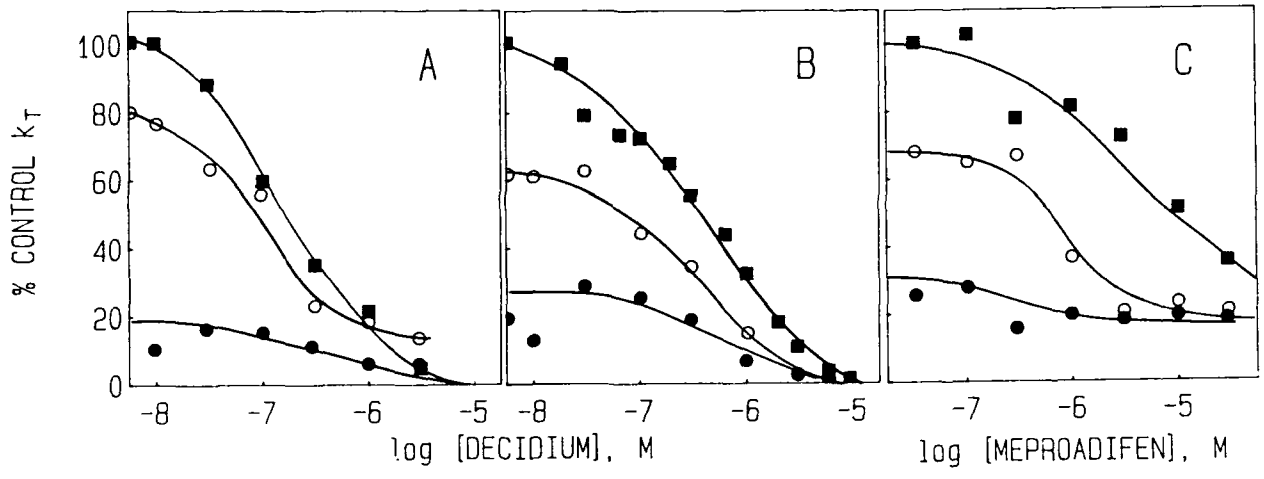

Fig. 22. Decidium modulation of [^{3}H]PCP binding to the *Torpedo* membranes.

Assays contained membranes (1 μM in α-toxin sites), [^{3}H]PCP (1 μM), plus specified effector ligand concentrations. ●-●, in the presence of carbachol (200 μM); △-△, in the presence of α-toxin (10 μM); ○-○, in the absence of both α-toxin and carbachol. Carbachol, α-toxin, and decidium were added 10 min before the addition of [^{3}H]PCP.

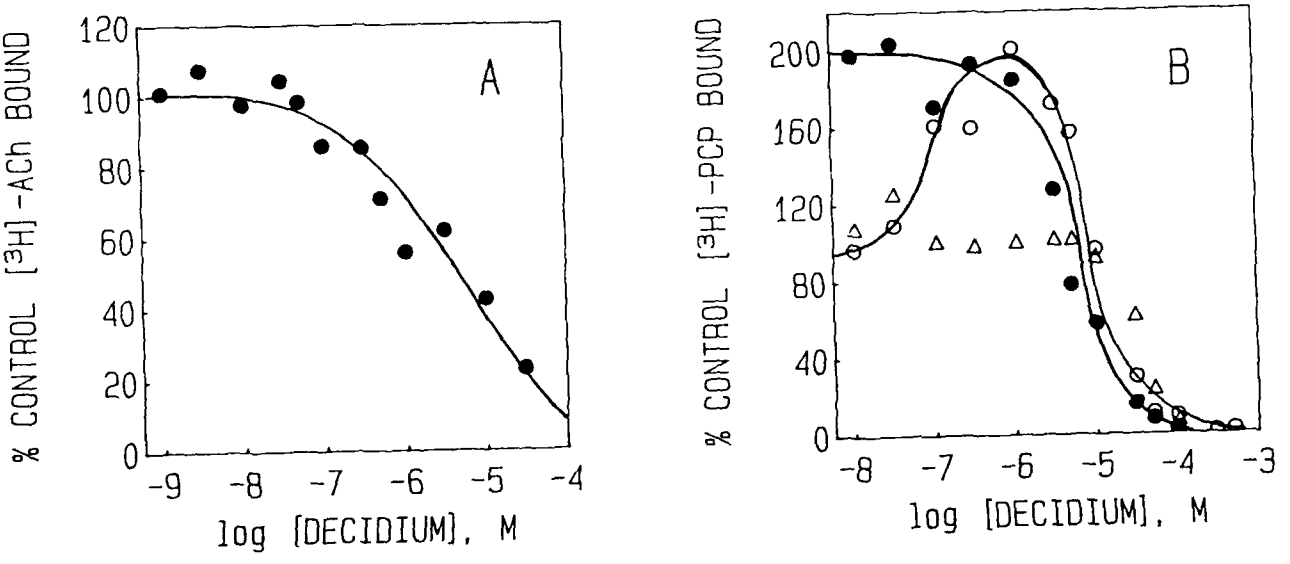

Fig. 23. (A) Normalized corrected-difference excitation spectrum of decidium bound to the membrane-enriched AcChR.

Dashed line represents the difference spectrum for decidium bound to the agonist sites obtained from samples (AcChR,0.25 μM in α-toxin sites; decidium, 1 μM; PCP, 100 μM) in the absence and presence of carbachol (500 μM). Solid line represents difference spectrum for decidium bound to the noncompetitive inhibitor site obtained from samples (AcChR, 1 μM in α-toxin sites; decidium, 2 μM; carbachol, 500 μM) in the absence and presence of PCP (100 μM). Dotted line represents the corrected emission spectrum of decidium in buffer. (B) Normalized uncorrected-difference emission spectrum of decidium bound to the membrane-enriched AcChR. Dashed line represents the difference spectrum for decidium bound to the agonist sites obtained from samples (AcChR, 0.25 μM in toxin sites; decidium, 1 μM; PCP, 100 μM) in the absence and presence of carbachol (500 μM). Solid line represents difference spectrum for decidium bound to the noncompetitive inhibitor site obtained from samples (AcChR, 1 μM in toxin sites; decidium, 2 μM; carbachol, 500 μM) in the absence and presence of PCP (100 μM). Dotted line represents the uncorrected excitation spectrum of decidium in buffer.

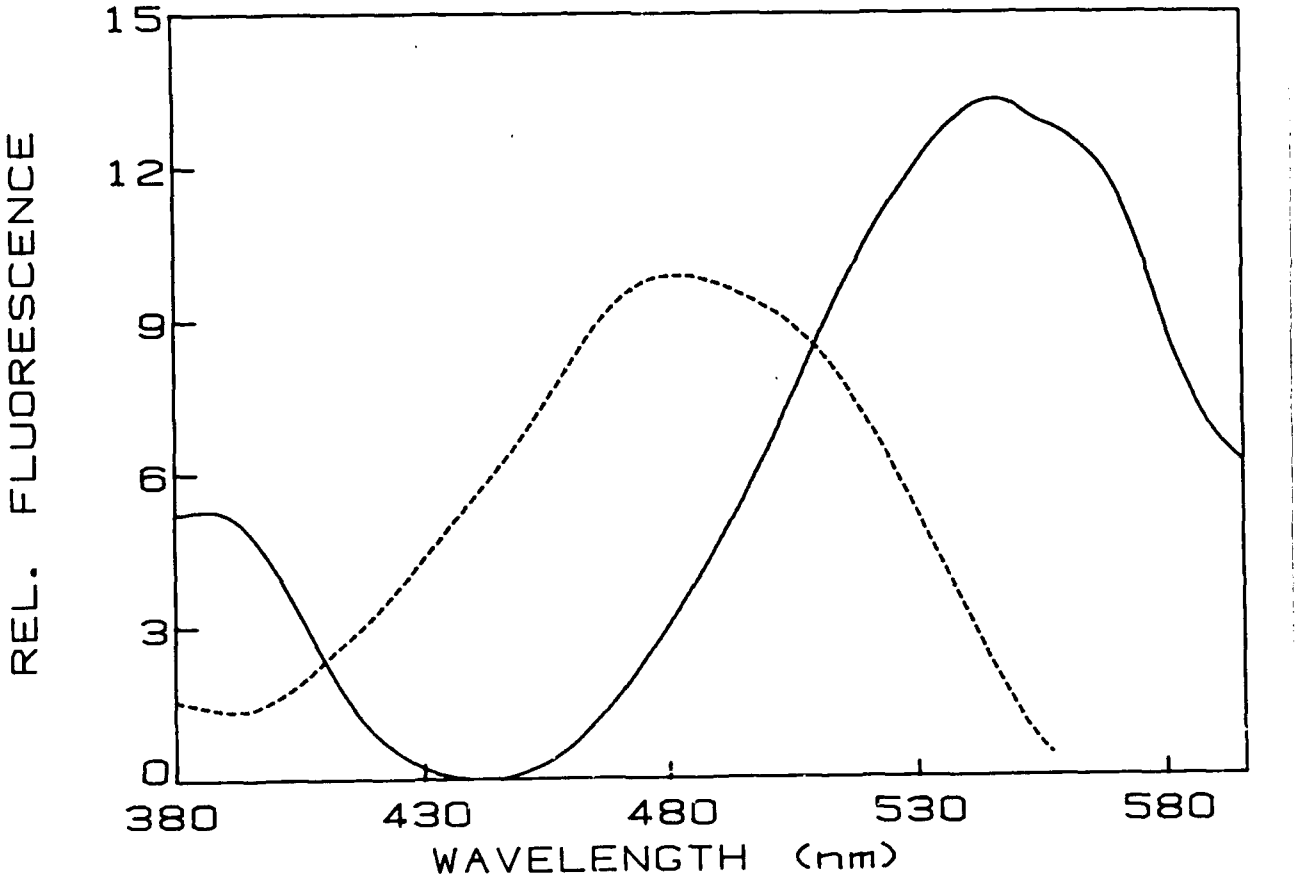

Fig. 24. (A) Titration of decidium with the membrane-enriched AcChR.

To 2.0 mL of membrane suspension of AcChR (0.2 μM in α-toxin sites) and 100 μM PCP were added incremental quantities of decidium. Fluorescence was measured at 620 nm with excitation at 290 and corrections made for dilution and inner filter effects. (a) □-□, membranes in the absence of α-toxin; (b) △-△, membranes in the presence of 2 μM α-toxin to define non-specific binding; (c) ●-●, buffer only. (B) Plot of specific enhancement of fluorescence as percentage of receptor bound versus the concentration of free ligand. The inset represents a Hill plot of this data.

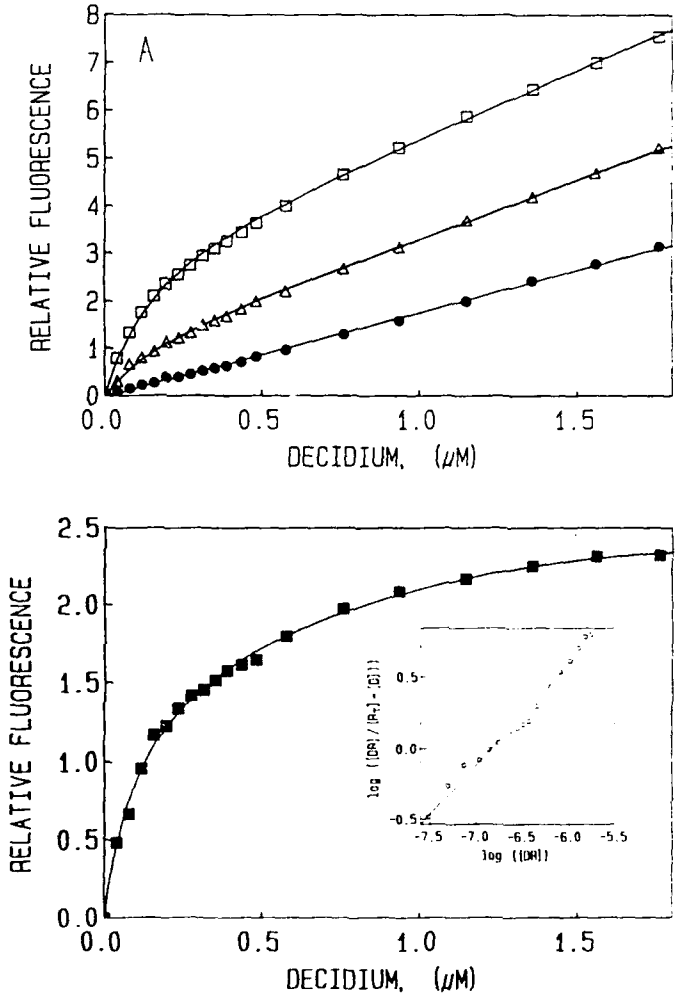

Fig. 25. Displacement titration of the decidium-AcChR complex by carbachol.

Panel A. Decidium (2.5 μM) was added to receptor-enriched membranes (0.25 μM in α-toxin sites), and incremental qualities of carbachol were added. Data were corrected for nonspecific fluorescence determined in a companion titration in the presence of excess α-toxin. Panel B. Plot of the displacement titration data ; f, f_B, and f_C represent the observed fluorescence, fluorescence with decidium alone, and fluorescence in presence of excess competing ligand. [B] and [C] are the estimated free concentrations of decidium and competing ligand, respectively.

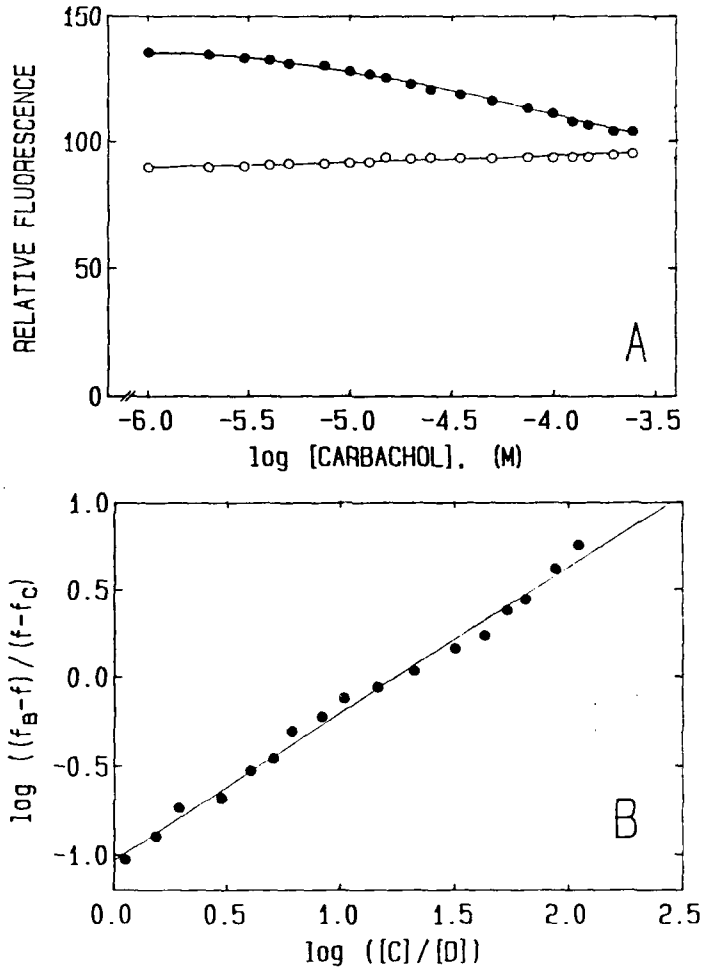

Fig. 26. Decidium quenching the fluorescence lifetime of FITC-toxin bound to the AcChR.

Nanosecond decay curves of FITC-toxin (0.6lM) were recorded in the presence of AcChR (4 μM in α-toxin sites), decidium (10 μM), and PCP (100 μM). The timing calibration was .43 ns/channel. Dashed lines represent the lamp pulse. Deviation of the experimental (data points) from a single exponential theoretical function (solid lines) are shown in the upper curves. AcChR is membrane-associated in Panels A and B and solubilized with 4% cholate in Panels C and D. In Panels B and D native α-toxin (10 μM) was incubated with the AcChR 30 min after the addition of FITC-toxin to inhibit decidium binding to th' agonist sites. Decidium was added to the sample cuvettes just before initiating the one hour data accumulation period. The data accumulation interval was limited to one hour in order to minimize the displacement of FITC-toxin from the agonist sites by decidium. The apparent decay curves generated from samples that did not contain FITC-toxin were subtracted from the AcChR samples to correct for light scatter.

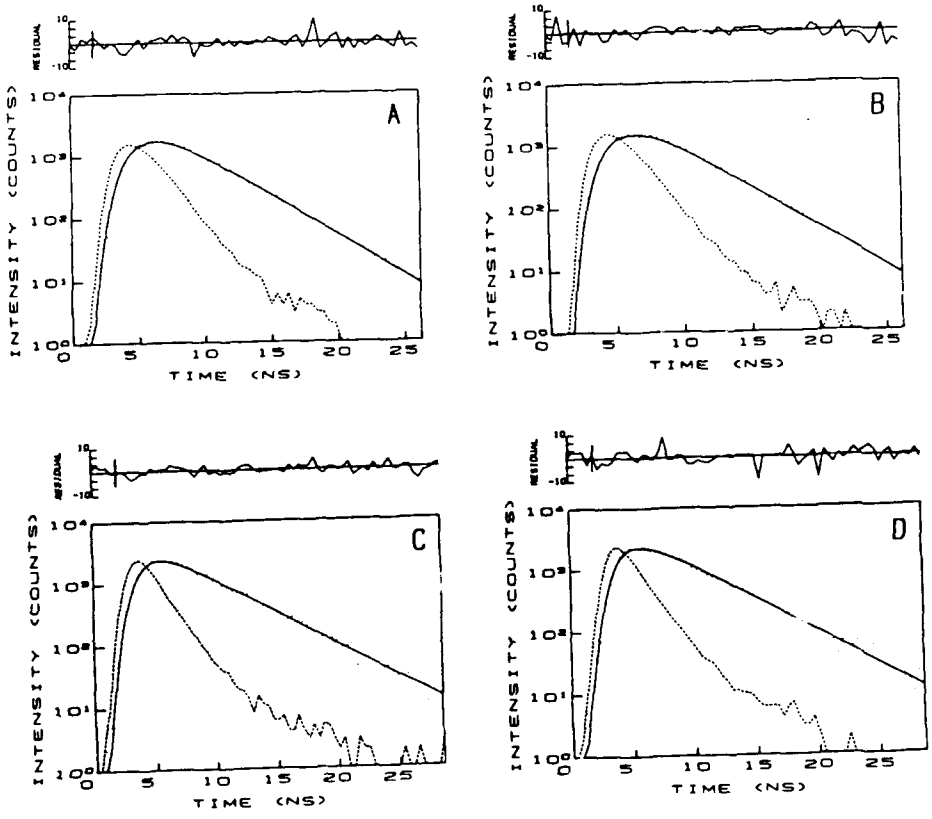

Table VII

Protection constants, K_p, for decidium inhibition of initial rates of carbachol-stimulated $^{22}Na^+$ influx and [^{125}I]labeled α-toxin binding. Effects of simultaneous or 30 min prior decidium exposure.

Inhibition data were obtained as described in Fig. 19. Data were analyzed as described by Sine and Taylor, 1979.

AcChR Source and Exposure Duration	K_p(M) ($^{22}Na^+$ influx)	n_H	K_p(M) ([^{125}I]-labeled α-toxin)	n_H
Intact BC3H-1 cells				
30 min	1.1×10^{-7}	0.89	4.4×10^{-7}	0.83
instantaneous	4.1×10^{-7}	0.75	9.0×10^{-7}	0.70
Torpedo membranes				
30 min	--	--	1.7×10^{-7}	0.84
instantaneous	--	--	2.9×10^{-7}	0.86

Table VIII

Nanosecond fluorescence decay of FITC-toxin bound to the AcChR (membrane-enriched and solubilized at 4.0 μM in α-toxin sites) in the presence and absence of decidium (10 μM).

PCP (100 μM) was present to block binding to the noncompetitive inhibitor site for PCP. In each case sufficient FITC-toxin (0.6 μM) was added to occupy 15% of the vacant sites. This decidium concentration (10 μM) should yield ~93% occupancy of the vacant sites.

	Lifetimes in ns ± S.D.(# of determinations)	
	Solubilized	Membrane-Enriched
FITC-toxin-AcChR	3.9±0.1 (2)	3.8±0.1 (2)
FITC-toxin-AcChR + decidium	3.8±0.1 (3)	3.2±0.2 (4)
FITC-toxin-AcChR +α-toxin-AcChR + decidium	3.8±0.1 (3)	3.2±0.2 (4)

SECTION VI

SPATIAL RELATIONSHIPS BETWEEN DRUG BINDING SITES AND ORIETATION OF TOXIN ON ACETYLCHOLINE RECEPTOR

Distance between agonist and high-affinity NCI sites. Our most recent work using two independent methods for measuring fluorescence energy transfer and by utilizing two different donor-acceptor pairsh as extended our understanding of the relative distances between the agonist/competitive antagonist sites and the high-affinity NCI site. 6-(5-Dimethyl-aminonapthalene-1-sulfamido)-hexanoic acid-β-(N-dimethyl-ammononium)ethyl (Dansyl-C_6-choline) [38], an agonist, and BCNI [37], a competitive antagonist, were employed as energy donors to the agonist/antagonists sites. Ethidium was employed as a specific probe of the NCI site [39] and served as the energy acceptor for either donor. Under steady-state conditions, energy transfer was measured by monitoring BCNI fluorescence as a function of acceptor occupancy. Changes in acceptor occupancy were achieved by titrating AcChR-donor-acceptor complexes with PCP, a nonfluorescent NCI ligand (see Fig. 27). Extrapolation of the data to 100% acceptor occupancy yielded a transfer efficiency of 38% for the BCNI-ethidium pair (see Fig. 28). In the second method, the transfer efficiency of the Dansyl-C_6-choline-ethidium pair was determined by analysis of the reduction of the donor excited state fluorescence lifetime. The decay of Dansyl-C_6-choline fluorescence measured in the presence of PCP is characterized by two lifetimes (τ_1=6.7 ns and τ_2=17.1 ns) with an amplitude ratio, a_1/a_2=2.3 (Fig. 29). In the presence of ethidium, the two lifetimes are diminished to 5.5 ns and 14.5 ns, while retaining a similar amplitude ratio. This suggests that the two lifetimes derive from the probe in two conformational states -- not two locations -- and is consistent with both donors bound to each of the two agonist sites transferring energy to the acceptor. Displacement of ethidium from the high-affinity NCI site by PCP restored the two lifetimes to their original values. The corrected efficiency of donor quenching by this method was 34%, which was in good agreement with the steady-state methods. The distance between each agonist site and the NCI site was calculated to be between 22 Å and 35 Å for the BCNI-ethidium pair and between 22 Å and 40 Å for the Dansyl-C_6-choline-ethidium pair. These studies delineate additional AcChR structural details and should contribute to our understanding of how agonists and antagonists modulate receptor function. Fig. 30 illustrates the distance relationships between the agonist/antagonist and NCI binding sites.

Fig. 27. Fluorescence emission spectra showing energy transfer between BCNI and ethidium bound to the AcChR.

AcChR-enriched membranes (0.4 μM in α-toxin sites) were incubated with the following ligands for 1 h at 25°C prior to a back titration with PCP. (A) BCNI (2 μM) and ethidium (1 μM); (B) carbachol (200μM) and ethidium; (C)BCNI, α-toxin (4 μM), ethidium. (D) shows the corresponding difference spectra of (A) minus (B). The numbered spectra correspond to PCP concentrations of 1) 0 μM, 2) 0.5 μM, 3) 1 μM, 4) 2 μM, 5) 4 μM, 6) 10 μM, 7) 50 μM.

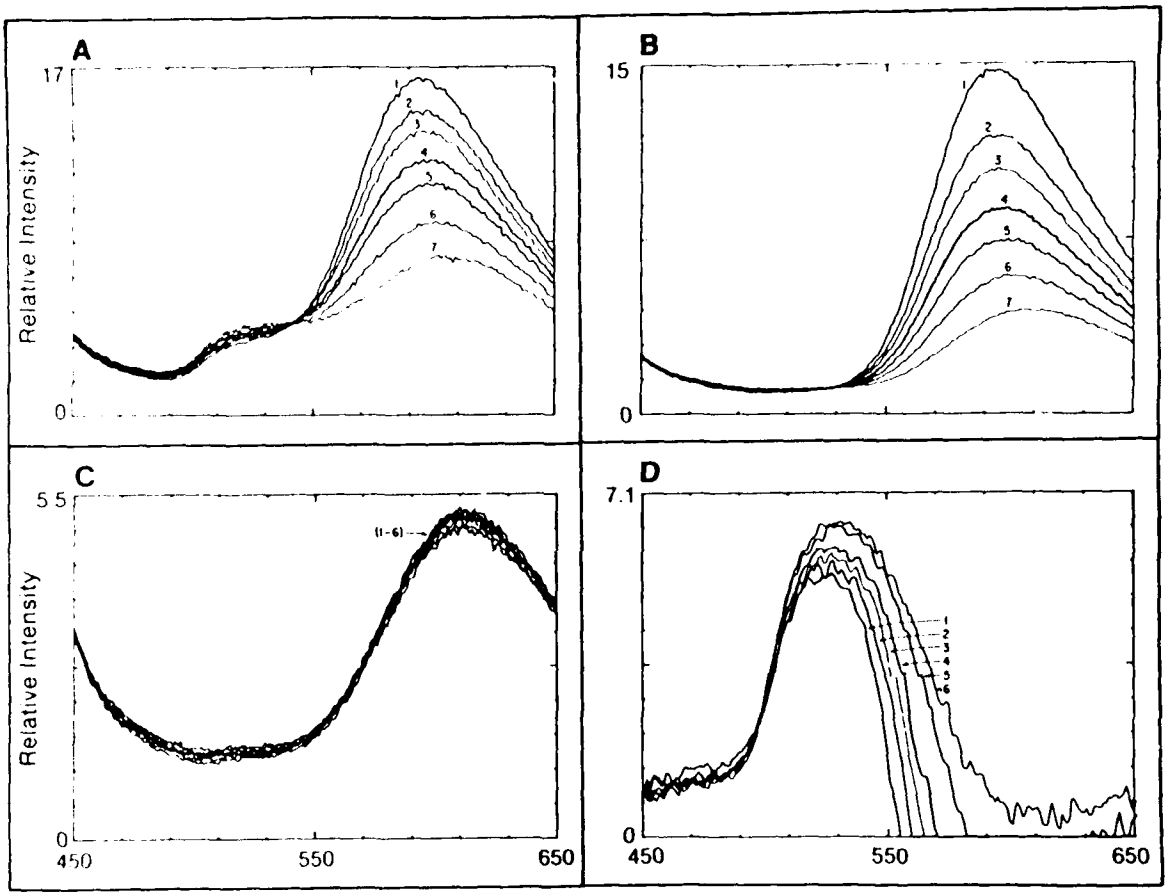

Fig. 28. Energy transfer efficiencies for BCNI-ethidium donor-acceptor pair at various acceptor occupancy levels.

A) Specific change in fluorescence intensity of BCNI (EM:525 nm) upon titration of PCP into AcChR-BCNI-ethidium complexes. The fluorescence increase reflects the loss of donor, BCNI, quenching due to displacement of the acceptor, ethidium, from the high-affinity NCI site. B) The observed transfer efficiencies plotted as a function of calculated ethidium occupation levels.

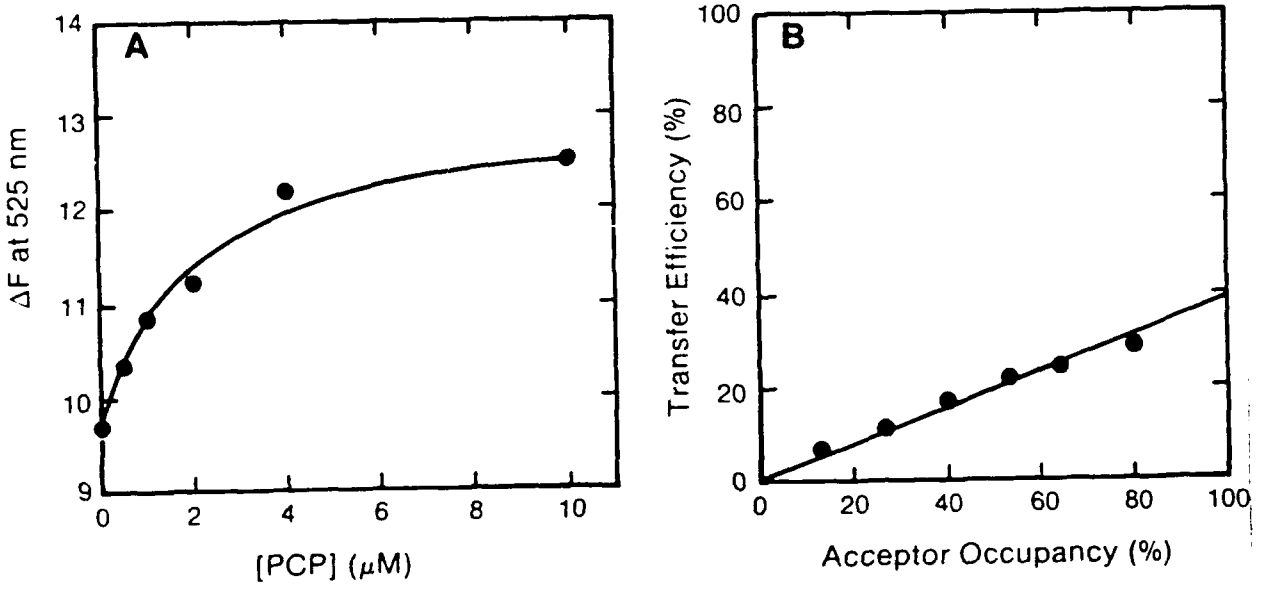

Fig. 29. Fluorescence decays showing energy transfer between dansyl-C_6-choline bound to the agonist site and ethidium bound to the high-affinity NCI site.

The double-exponential decay of dansyl-C_6-choline (1 μM) obtained in the presence of AcChR-enriched membranes (1 μM in α-toxin sites) and (A) ethidium (1 μM) or (B) ethidium (1 μM) and PCP (200 μM). Each panel shows lamp pulse (dashed lines), experimental points (dots), computer fit (solid line), and weighted residuals plots above each decay plot.

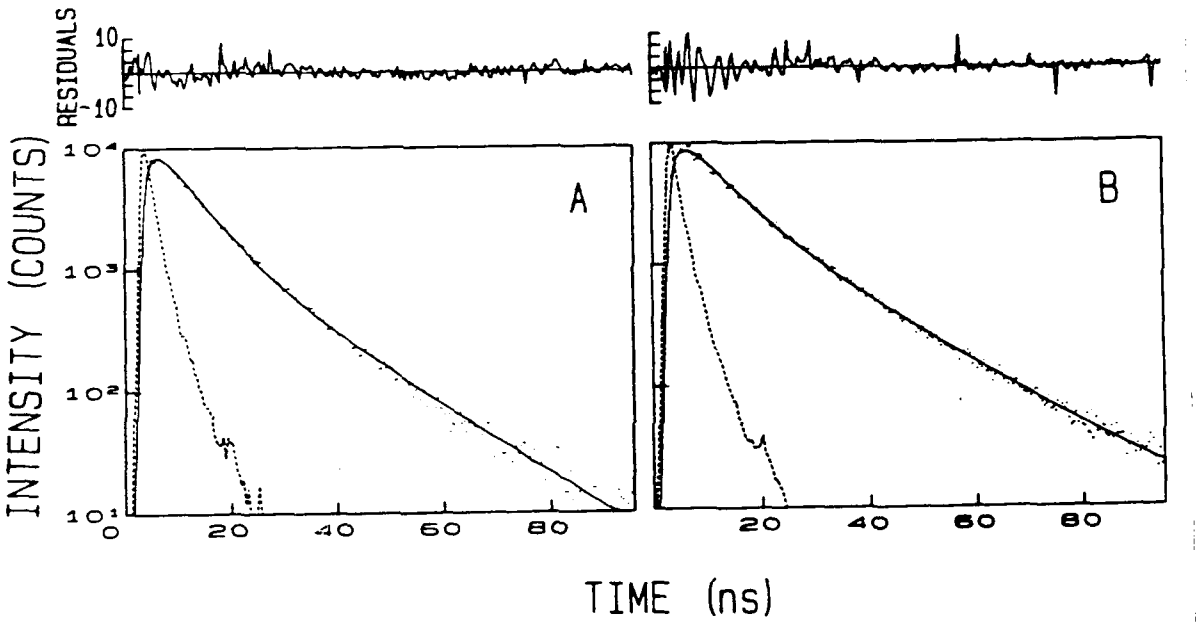

Fig. 30. Model of acetylcholine receptor structure showing possible locations for agonist and NCI sites.

The molecular dimensions and overall shape of the AcChR are based upon the data of Unwin [70, 71]. The average agonist-NCI intersite distance of 30 Å determined in this study is drawn to scale. The two agonist sites are positioned symmetrically with respect to the central axis of the AcChR. The inner and outer lateral limits of the agonist boxes define agonist-agonist intersite distances of 30 Å and 50 Å, respectively, while the vertical limits are 20 Å and 26 Å from the synaptic membrane surface. Unresolved dimensions of the AcChR for which there are no accurate data are denoted by dashed lines.

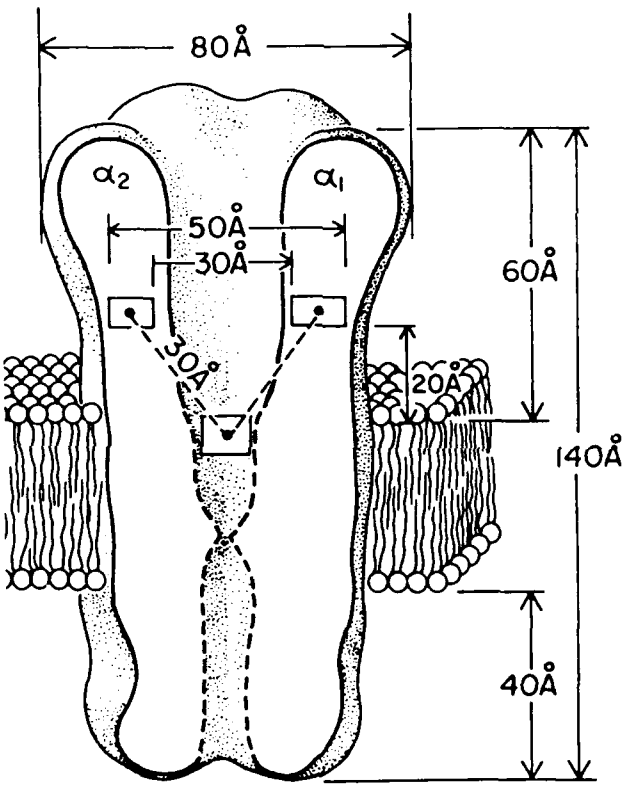

Orientation of α-toxin on AcChR. We have recently extended research on the disposition of α-neurotoxins bound to the receptor to allow a delineation of the orientation of α-toxin on the receptor. We examined four aspects of the interaction of fluorescein-labeled α-toxin bound to the receptor. First, we measured the accessibility of iodine to the fluorescein conjugated to lys 23, lys 35, lys 49, or lys 69 on *siamensis 3* α-toxin bound to the receptor and found all four sites nearly equally accessible (see Table IX). Second, we examined the capacity of the receptor tryptophans to transfer energy to the above-mentioned fluorescein α-toxin derivatives and found that the FITC-lys 49 derivative was much more likely to accept energy from receptor tryptophans than were the other derivatives (Table X). There are more than 40 tryptophans in the extracellular domain of the receptor and energy transfer is occurring from more than one donor-acceptor pair. If we assume uniform distribution of tryptophans, these results suggest that lys 49 of the bound α-toxin is closer to the receptor than lys 23, lys 35, or lys 69. Third, we assessed the apparent energy transfer efficiency between a tetramethylrhodamine (TRITC)-lys 23-α-toxin and the above mentioned FITC α-toxin derivatives and found that when the FITC and TRITC derivatives are bound to separate α-toxin binding sites on the same receptor, Lys 23 on one α-toxin is closer to Lys 35 on the other bound α-toxin (see Table XI). Finally, we estimated, using energy transfer techniques, the distance of closest approach between the above-mentioned fluorescein derivatives and 5-(N-docecanoylamino-eosin (C_{12}-eosin) intercalated into the lipid bilayer. We observed that, when bound to the receptor, lys 23 (40 Å) and lys 49 (41 Å) are closer to the surface of the membrane than are lys 35 (46 Å) and lys 69 (46 Å) (see Fig. 31 and Table XII). These four lines of evidence, combined with the known tertiary structure of the α-toxin [49] and the previous research establishing the central loop of α-neurotoxin to be in contact with the receptor, allow us to sketch the orientation of the α-toxin on the receptor. The α-neurotoxins rest on the receptor with the regions of the α-toxin near lys 23 and lys 49 nearer to perimeter of the receptors as shown in Fig. 32.

Table IX.

Bimolecular potassium iodide quenching rate constants of fluorescein free in solution and FITC α-toxin derivatives conjugated to lys, 23, lys 35, lys 49, or lys 69 free in solution and bound to the membrane-associated AcChR. The rate constants were calculated by dividing the measured Stern-Volmer quenching constants (k_Qs) by the measured fluorescence lifetimes (data not shown). The standard deviations range between 0.02 and 0.05.

Bimolecular Quenching Rate Constants (k_{FQ}s)

Fluorophore	Free in solution ($1x10^9$ s^{-1})	Bound to AcChR ($1x10^9$ s^{-1})
FITC-Lys 35-toxin	1.40	1.05
FITC-Lys 69-toxin	1.37	1.22
FITC-Lys 49-toxin	1.57	1.06
FITC-Lys 23-toxin	1.60	1.04
Fluorescein	3.19	

Table X.

Relative energy transfer between AcChR tryptophans and FITC conjugated to lys 23, lys 35, lys 49, or lys 69 on the cobra α-toxin (20 nM) bound to the AcChR (10-100 nM in α-toxin sites). The relative energy transfer was measured by quantitation of the change in FITC fluorescence associated with binding of the above-mentioned derivatives to the AcChR upon excitation of either the tryptophan (EX: 280 nm) or FITC (EX: 480nm). Dividing the binding-dependent change in fluorescence with excitation of the tryptophans by the binding-dependent change with direct excitation of the FITC (EX:280/EX:480) yields an estimate of the relative energy transfer between receptor tryptophans and the FITC conjugated to specified sites on the receptor-bound α-toxins. The standard deviations range between 0.01 and 0.13.

Change in Steady State Fluorescence upon Binding

Derivatives	Bound/Free (EX:480)	Bound/Free (EX:280)	(EX:280/ EX:480)
FITC-Lys 35-toxin	0.61	1.22	2.01
FITC-Lys 69-toxin	0.73	1.52	2.10
FITC-Lys 49-toxin	0.95	2.97	3.11
FITC-Lys 23-toxin	1.96	4.28	2.18

Table XI.

Energy transfer between FITC-toxin derivatives (0.5 μM) (conjugated at lys 23, lys 35, lys 49, or lys 69) bound to one of the two α-toxin sites and TRITC-lys 23-α-toxin (2 μM) which is bound to the other site on the same triton-X100 solubilized (but not denatured) AcChR (2 μM in α-toxin sites). Shown are the donor quantum yields, Q_D, the critical distances for each donor-acceptor pair (Forster critical distance), R_o, the measured % transfer efficiencies, E_A, and the calculated distance, R.

Donor FITC at	Q^D	R_0, Å	E_A, %	R, Å
Lys 23	0.35	46.7	0.0	< 100
Lys 35	0.19	42.3	5.3	68
Lys 49	0.36	47.2	1.3	77
Lys 69	0.30	46.0	2.0	88

Fig. 31. Energy transfer between FITC site specifically conjugated to α-toxin (50 nM) bound to the AcChR (100 nM in α-toxin sites) and C_{12}-eosin intercalated into the lipid bilayer.

Shown are FITC α-toxin derivatives conjugated to lys 23, lys 35, lys 49 or lys 69. These derivatives are bound to the membrane-associated AcChR (filled circles) or prevented from binding by prior exposure of the receptor to excess native α-toxin (open circles). For comparison, C_{12}-eosin is titrated into AcChR samples in which fluorescein-C_{12}-acylamide had been allowed to intercalate into the bilayer. The donor, fluorescein, fluorescence in the absence (I_o) and presence of various concentrations of acceptor, C_{12}-eosin, (I) is plotted as a function of C_{12}-eosin concentrations.

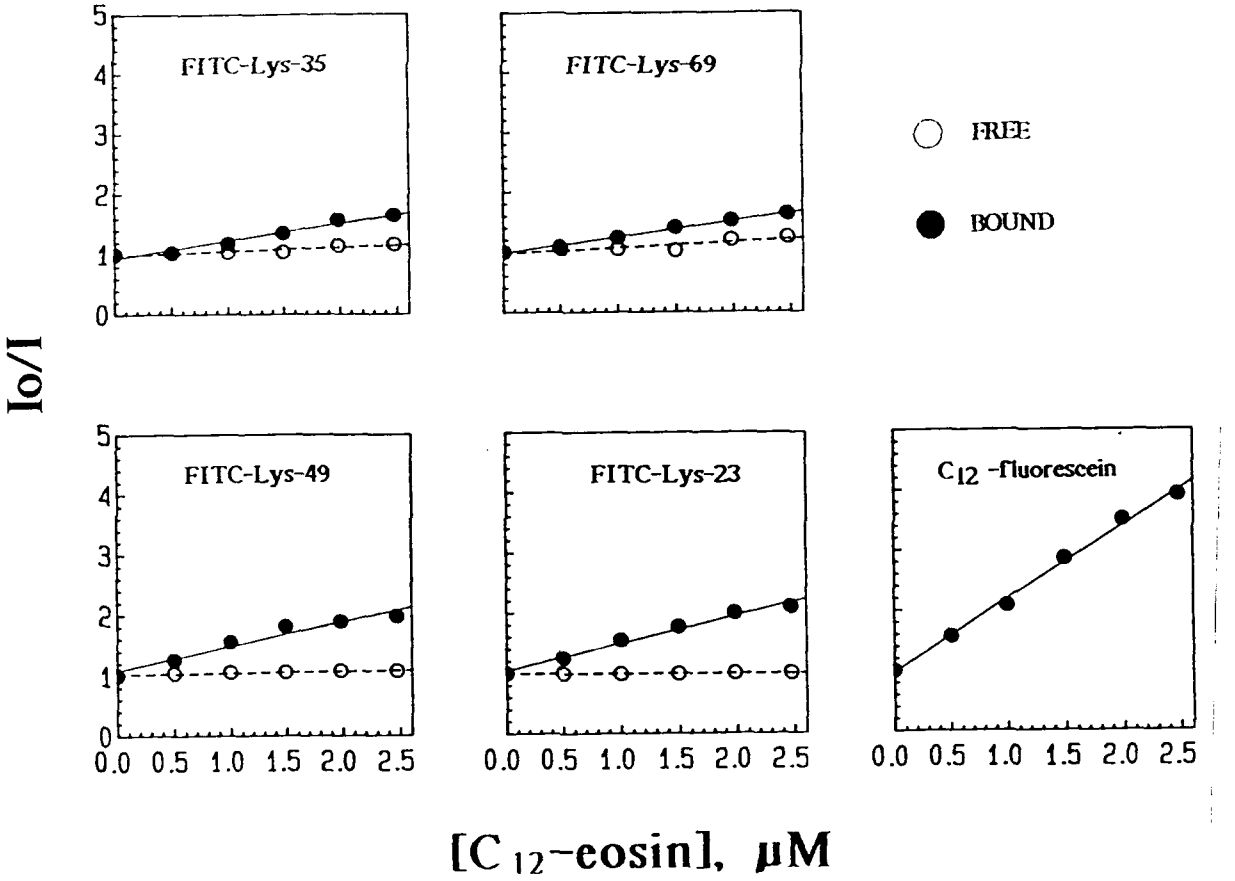

Table XII

Summary of Energy Transfer Parameters for donor fluorescein derivatives and acceptor, C_{-12}-eosin.

Donor	Acceptor	ϵ_A[d]	J[e]	R_o[f]	K[g]	L[h]
		($M^{-1}cm^{-1}$)	cm^6 mol	Å	$x10^{-5}M$	Å
FITC-lys-23-toxin	C_{12}-eosin	85,000[c]	$2.94x10^{-13}$	45.8	4.7±03	40
FITC-Lys-35-toxin	C_{12}-eosin	85,000[c]	$3.09x10^{-13}$	41.6	2.2±0.3	45
FITC-Lys-49-toxin	C_{12}-eosin	85,000[c]	$3.16x10^{-13}$	46.4	3.8±0.5	41
FITC-Lys-69-toxin	C_{12}-eosin	85,000[c]	$3.13x10^{-13}$	45.1	1.7±0.1	46
5-(dodecanoylamino) fluorescein	C_{12}-eosin	85,000[c]	$3.03x10^{-13c}$	50.1[c]	12.2±0.5	

[a]Quantum yield. [b]Q_D was calculated by multiplying the quantum yield of the free derivative by the fractional change of fluorescence with direct excitation (Ex: 480 nm) upon binding from data determined elsewhere [49]. [c]Values from [72]. [d]Molar extinction at maximum visible wavelength. [e]Overlap integral. [f]Forster critical distance (assumptions: $\kappa 2 = 2/3$ and $n = 1.6$). [g]K, specific slope of Q_D/Q_{DA} versus C_{12}-eosin plots in Fig. 31. [h]Calculated distance of closest approach between C12-eosin on the surface of the lipid membrane and the site of FITC derivatization on the AcChR-bound α-toxin (see [54]).

Fig. 32. Model of the orientation of the cobra-α-toxin bound to the AcChR.

The ellipsoidal α-toxin sits on the top of the receptor with its major axis tilting slightly from a perpendicular membrane projection. The various sites of FITC labeling are shown approximately at the tip of the numbered triangles and are based on the X-ray coordinates of the native α-toxin [48].

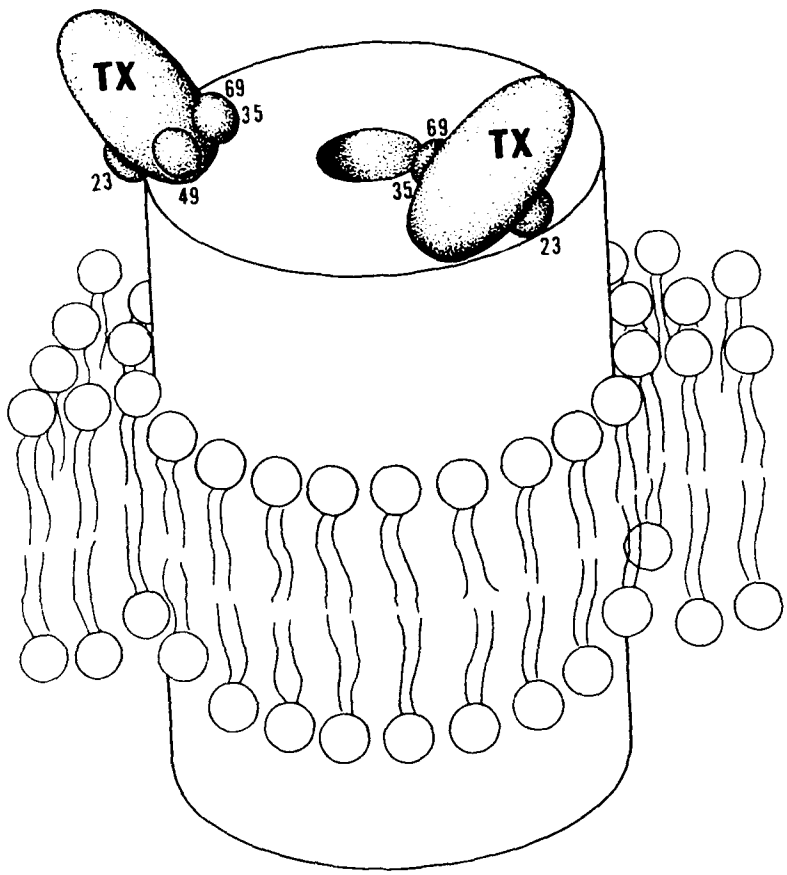

BIBLIOGRAPHY

1. Lester, H.A., J.P. Changeux and R.E. Sheridan. 1975. J. Gen. Phys., 65:797.
2. Karlin, A. 1980. In: Cell Surface and Neuronal Function (Cotman, Poste and Nicolson, eds.), Vol. 5, pp. 191-256, Elsevier/North Holland, New York.
3. Taylor, P., R.D. Brown and D.A. Johnson. 1982. In: Current Topics in Membrane Receptors and Transport (A. Kleinzeller, ed.), Vol. 18, Ch. 15, pp. 407-443.
4. Weiland, G., B. Georgia, V.T. Wee, C.F. Chignell and P. Taylor. 1976. Mol. Pharmacol., 12:1091.
5. Weill, C.L., M.G. McNamee and A. Karlin. 1974. Biochem. Biophys. Res. Commun., 61:997-1003.
6. Raftery, M.A., R.L. Vandlen, K.L. Reed and T. Lee. 1975. Sym. Quant. Biol., 40:193-202.
7. Damle, V., M. McLaughlin and A. Karlin. 1978. Biochem. Biophys. Res. Commun., 84:845-851.
8. Noda, M., H. Takahashi, T. Taube, M. Toyosata, Y. Furutani, T. Hirose, M. Asai, S. Inayam, T. Miyata and S. Numa. 1982. Nature (Lond.), 299:793-797.
9. Noda, M., H. Takahashi, T. Taube, M. Toyosato, S. Kikyotani, t. Hirose, M. Asai, H. Takashima, S. Inayam, T. Miyata and S. Numa. 1983. Nature (Lond.), 301:251-255.
10. Claudio, T., M. Ballivet, J. Patrick and S. Heinemann. 1983. Nature (Lond.), 80:1111-1115.
11. Neubig, R.R., E.K. Krodel, N.D. Boyd and J.B. Cohen. 1979. Proc. Natl. Acad. Sci. USA, 76:690-694.
12. Ross, M.J., M.W. Klymkowsky, D.A. Agard and R.M. Stround. 1977. J. Membr. Biol., 116:635-639.
13. Raftery, M.A., J. Schmidt and D.G. Clark. 1972. Arch. Biochem. Biophys., 152:882-886.
14. Changeux, J.-P., E.L. Bendetlig, J.-P. Bourgeois, A. Brusson, J. Cartaud, P. Devaux, H. Grunhagen, M. Moreau, J.-L. Popot, A. Sobel and M. Weber. 1979. Symp. Quant. Biol., 40:211-230 umbrella.
15. Eldefrawi, M.E., A.T. Eldefrawi, N.A. Mangour, J.W. Daly, B. Witkop and E.X. Albuquerque. 1978. Biochemistry, 17: 5475-5484.
16. Krodel, E.K., R.A. Beckmann and J.B. Cohen. 1979. Mol. Pharmacol., 15:294-312.
17. Sator, V., J.M. Gonzalez-Ros, P. Galuo-Fernandez and M. Martinez-Carrion. 1979. Biochemistry, 18:1200-1206.
18. Zingsheim, H.P., F.J. Barrantes, J. Frantz, W. Hanicke and D.Ch. Neugebauer. 1982. Nature, 299:81-84.
19. Johnson, D.A. and P. Taylor. 1982. J. Biol. Chem., 257:5632-5636.
20. Johnson, D.A., J. Voet and P. Taylor. 1983. J. Biol. Chem., 259:5717-5725.
21. Boyd, N.D. and J.B. Cohen. 1984. Biochemistry, 23:4023-4033.
22. Blanchard, S.G., J. Elliott and M.A. Raftery. 1979. Biochemistry, 18:5880-5885.
23. Brisson, A. and P.N.T. Unwin. 1985. Nature, 315:474-477.
24. Changeux, J.-P., Giraudat, J., and Dennis, M. (1987) Trends Pharmacol. Sci., 8, 459-465.
25. Kao, P.,Dwork, A., Kaldany, R., Silver, M., Wideman, J.,Stein, S., and Karlin, A. (1984) J. Biol. Chem., 259, 11662-11665.
26. Hucho, F., Oberthür, W. and Lottspeich, F. (1986) FEBS Lett., 205, 137-142.
27. Giraudat, J., Dennis, M., Heidmann, T., Chang, J.-Y., and Changeux, J.-P. (1986) Proc. Natl. Acad. Sci. USA, 83, 2719-2723.
28. Giraudat, J., Dennis, M., Heidmann, T, Haumount, P.-Y., Lederer, F., and Changeux, J.-P.

(1987) Biochemistry, 26, 2410-2418.
29. Delgeane, A.M. and McNamee, M.G. (1980) Biochemistry, 19, 890-895.
30. Johnson, D.A., Brown, R.D., Herz, J.M., Berman, H.A., Andresen, G.L., and Taylor,P., (1987) J. Biol. Chem., 262, 14022-14029.
31. Noda, M., H. Takahashi, T. Taube, M. Toyosato, S. Kikyotani, t. Hirose, M. Asai, H. Takashima, S. Inayam, T. Miyata and S. Numa. (1983), 302, 528-532.
32. Guy, H. R. (1984) Biophys J., 45, 249-261.
33. Finer-Moore, J. and Stroud, R.M. (1984) Proc. Natl., Acad Sci., USA, 81, 155-159.
34. Linstrom,. (1986) Trends Neurosci., 9, 401-407.
35. Adams. P.R. (1976) J. Physiol. London, 260, 531-552.
36. Neher, E. and Steinbach, J.H. (1978) J. Physiol. London, 227, 153-176.
37. Bolger, M.B., Dionne, V., Chriva, J., Johnson, D.A., and Taylor, P. (1984) Mol. Pharmacol., 26, 57-69.
38. Waksman, G., Changeau, J-P., and Roques, B.P. (1980) Mol. Pharmacol., 18, 20-27.
39. Herz, J., Johnson, D.A., and Taylor, P. (1987) J. Biol. Chem., 262, 7238-7247.
40. Lobel, P., Koa, P.N., Birken, S., and Karlin, A. (1985) J. Biol. Chem., 260, 10605-10612.
41. Ralston, S., Sarin, V., Thanh, H.L., River, J., Fox, J.L., and Lindstrom, J. (1987) Biochemistry, 26, 3261-3266.
42. Lentz, T.L., Hawrot, E., and Wilson, P.T. (1987) Proteins, 2, 298-307.
43. Dufton, M.J. and Hider, R.C. (1988) CRC Crit. Rev. Biochem., 14, 113-171.
44. Garcia-Borron, J-C., Bieber, A.L. and Martinez-Carrion, M. (1987) Biochemistry, 26, 4295-4303.
45. Martin, B.M., Chibber, B.A., and Maelicke, A. (1983) J. Biol. Chem., 258, 8714-8722.
46. Balsubramaniam, K., Kaker, D., and Karlsson, E. (1983) Toxicon, 21, 219-229.
47. Bystrov, V.F., Tsetlin, V.I., Karlsson, E., Pashkov, V.S., Utkin, Y., Kondakov, V.I., Pluzhnikov, K.A., Arseniev, A.S., Ivanov, V.T., and Ovchinnikov, Y. A., (1983) in Toxins as Tools in Neurochemistry (Hucho, F. and Orchinnikov, Y.A. eds) pp 171-191, Walter de Gruyter and Co., New York.
48. Walkinshaw, M.,D., Saenger, W., and Maelicke, A. (1980) Proc. Natl., Acad. Sci, 77, 2400-2404.
49. Johnson, D.A. and Cushman, R. (1988) J. Biol. Chem., 263, 2802-2807.
50. Heidmann, T., R.E. Oswald and J.-P. Changeux. 1983. Biochemistry, 22:3112-3127.
51. Karlin, A. (1987) Nature, 239, 286-7.
52. Kubalek, E., Ralston, S., Lindstrom, J., and Unwin, N. (1987) J. Cell Biol. 105, 9-18.
53. Johnson, D.A. and Cushman, R. (1988) J. Biol. Chem. 263, 2802-2807.
54. Johnson, D.A,, Cushman, R., and Malekzadeh, R. (1990) J. Biol. Chem. 265, 7360-7368.
55. Cheung, A.T., Johnson, D.A., and Taylor, P., 1984. Biophys. J. 45, 447-454.
56. Parker, C.A. and Rees, W.T. (1960 Analyst, 85, 587.
57. Weiland, G.A., Georgia, B., Lappi, S., Chignell, C. F., and Taylor, P. (1977) J. Biol. Chem. 252, 7648-7656.
58. Krodel, E.K., Beckman, R.A. and Cohen, J.B. (1979) Mol. Pharmacol. 15, 294-312.
59. Weiland, G.A. and Taylor, P. (1979) Mol. Pharmacol., 15, 197-212.
60. Olmsted, J. III and Kearns, D.R. (1977) Biochemistry 16:3647-3654.
61. Neubig, R.R. and Cohen, J.B. (1979) Biochemistry, 18, 5464-5474.
62. Sine, S.M. and Taylor, P. (1981) J. Biol. Chem., 256, 6692-6699.
63. Rang, H.P. and Ritter, J.M. (1970a) Mol. Pharmacol., 6, 357-382.
64. Rang, H.P. and Ritter, J.M. (1970b) Mol. Pharmacol., 6, 383-390.
65. Sine, S.M. and Taylor,P. (1980) J. Biol. Chem., 255, 10144-10156.
66. Boyd, N.D. and Cohen, J.B. (1980) Biochemistry 19, 5344-5353.
67. Quast, U., Schimerlik, M., Lee, T., Witzemann, V., Blanchard, S. and Raftery, M.A. (1978)

Biochemistry 17, 2405-2415.
68. Albuquerque, E.X., Tsai, M-C., Aronstan, R., Witkop, B., Eldefrawi, A.T., Eldefrawi, M. E. (1980) Mol. Pharmacol., 18, 159-178.
69. Palma, A., Herz, J.M., Wang, H.H. and Taylor, P. (1986) Mol. Pharmacol. 30, 243-251.
70. Unwin, N., Toyoshima, C., and Kubalek, E. (1988) J. Cell Biol. 107, 1123-1138.
71. Toyoshima, C. and Unwin, N. (1988) Nature, 338, 247-2500.
72. Holowka, D. and Baird, B. (1983a) Biochemistry 22, 3466-3474.

BIBLIOGRAPHY OF ALL PUBLICATIONS SUPPORTED BY THE CONTRACT

1. Taylor, P., P. Culver, R.D. Brown, J. Herz and D.A. Johnson. 1985. An Approach to Anesthetic Action from Studies of Acetylcholine Receptor Function. In: Molecular Mechanisms of Anesthesia, Vol. III, pp.99-110, K.W. Miller and S. Roth, Ed., Plenum Press.
2. Johnson, D.A. and J. Yguerabide. 1985. Solute Accessibility to N^{ϵ}-Fluorescein Isothiocyanate-Lysine-23-Cobra α-Toxin Bound to the Acetylcholine Receptor: A consideration of the Effect of Rotational Diffusion and Orientational Constraints on Fluorescence Quenching: Biophys. J. 48:949-955.
3. Taylor, P., J.M. Herz, D.A. Johnson and R.D. Brown. 1986. Topography of the Acetylcholine Receptor Revealed by Fluorescence Energy Transfer. In: Mechanism of Action of Nicotinic Acetylcholine Receptor, pp. 61-74, A. Maelicke, Ed. Springer-Verlag.
4. Herz, J.M., D.A. Johnson and P. Taylor. 1987. Interaction of Noncompetitive Inhibitors with the Acetylcholine Receptor: The Site and Specificity of Ethidium Binding. J. Biol. Chem. 262:7238-7247.
5. Johnson, D.A., R.D. Brown, J.M. Herz, H.A. Berman, G.L. Adreasen and P. Taylor. 1987. Decidium: A novel fluorescent probe of the agonist/antagonist and noncompetitive inhibitor sites on the nicotinic acetylcholine receptor. J. Biol. Chem. 262:14022-14029.
6. Johnson, D. and R. Cushman. 1988. Purification and characterization of four mono-fluorescein cobra-α-toxin derivatives. J. Biol. Chem. 263:2802-2807.
7. Herz, J., Johnson, D.A., and Taylor, P. (1989) Distance between the agonist and noncompetitive inhibitor sites on the nicotinic acetylcholine receptor. J. Biol. Chem. 264, 12439-12448.
8. Johnson, D.A,, Cushman, R., and Malekzadeh, R. (1990) Orientation of cobra α-toxin on the surface of the nicotinic acetylcholine receptor: Fluorescence Studies. J. Biol. Chem. 265, 7360-7368.

LIST OF PERSONNEL RECEIVING CONTRACT SUPPORT

David A. Johnson, Ph.D., P.I.
Rosemary Cushman (Staff Research Assistant)
Anthony E. Cheug (undergraduate student)
Lan Nguyen (undergraduate student)
David Kaiser (undergraduate student)
Walter Andrada (undergraduate student)
John Azvedo (Received M.A. Degree in Biology 12/88)
Timothy Jolliff (undergraduate student)

LIST OF ABBREVIATIONS

ACh	Acetylcholine
AcChR	Nicotinic Acetylcholine Receptor
α-toxin	Cobra α-toxin (*Naja naja siamensis 3*)
IEF	Isoelectric Focusing
pI	Isoelectric Focusing Point
NP buffer	100 mM NaCl, 10 mM NaPO4, pH 7.4
σ	surface density as number of acceptors/Å2.
BCNI	bis-(choline)N-[4-nitrobenzo-2-oxa-1,3-diazol-7-yl] -iminodiproprionate
C_{12}-eosin	5-(N-dodecanoylamino)-eosin
C_{12}-fluorescein	5-(N-dodecanoylamino)-fluorescein
Dansyl-C_{12}-Choline	6-(5-dimethylaminonapthalene-1-sulfamido)-hexanoic acid-β-(N-rimethylammonium) ethyl ester
Eff	energy transfer efficiency
FITC	fluorescein isothiocyanate
FITC-lys-23-toxin	$N_e$fluorescein-lysine-23-α-toxin
FITC-lys-35-toxin	$N_e$fluorescein-lysine-35-α-toxin
FITC-lys-49-toxin	$N_e$fluorescein-lysine-49-α-toxin
FITC-lys-69-toxin	N^efluorescein-lysine-69-α-toxin
HTX	histriionicotoxin
J	overlap integral
κ^2	orientation factor
k_{FQ}	bimolecular quenching rate constant
K_Q	Stern-Volmer quenching constant;
L	Transverse distance between lipid-membrane surface and AcChR-bound fluorophore
MBTA	4-(n-maleimidophenyl)-[^{3}H]-trimethyl ammonium
NCI	noncompetitive inhibitor
PCP	phencyclidine
Q	quantum yield
Q_D	donor quantum yield
Q_{DA}	donor quantum yield in presence of acceptor
R_o	Forster critical distance
TRITC	tetramethylrhodamine isothiocyanate

DISTRIBUTION LIST

1 Copy	Commander US Army Research and Development Command ATTN: SGRD-RMI-S Fort Detrick, Frederick, Maryland 21701-5012
5 Copies	Commander US Army Medical Research and Development Command ATTN: SGRD-PLE Fort Detrick, Frederick, Maryland 21701-5012
2 Copies	Defense Technical Information Center (DTIC) ATTN: DTIC-FDAC Cameron Station Alexandria, VA 22304-6145
1 Copy	Dean School of Medicine Uniform Services University of the Health Sciences 4301 Jones Bridge Road Bethesda, MD 20814-4799
1 Copy	Commandant Academy of Health Sciences, US Army ATTN: AHS-CDM Fort Sam Houston, TX 78234-6100